SYSTEM DESIGN AND ANALYSIS METHODS FOR OPTIMAL ELECTRIC VEHICLE THERMAL MANAGEMENT

BY

SAGAR SINGH

THESIS

Submitted in partial fulfillment of the requirements
for the degree of Master of Science in Mechanical Engineering
in the Graduate College of the
University of Illinois Urbana-Champaign, 2023

Urbana, Illinois

Adviser:

Professor Nenad Miljkovic

ABSTRACT

The thermal management system (TMS) in an electric vehicle (EV) encounters many challenges due to the stringent thermal requirements of EV components and concurrent range reduction in cold conditions. Efficient systems require thermal architectures with highly interconnected components to satisfy a wide range of operating conditions. A need exists to develop a methodology which can enable analysis-driven design decisions by leveraging a simulation framework to capture dynamic physical interactions. Here, a versatile simulation framework is developed inside MATLAB-Simulink using Simscape for transient analysis of coolant and refrigerant thermal systems and is validated at both the component and system-levels. A decision tree for EV TMS design is developed to evaluate various trade-offs. Direct and indirect configurations for cabin conditioning are analyzed to compare relative performance. The indirect configuration is found to have a 1.6-1.8x longer conditioning time and a coefficient of performance (COP) decrease of 18-31% and 31-41% for heating and cooling, respectively. A previously unexplored general integrated loop architecture is formulated for concept-level analysis of various EV TMS configurations. Operating modes are formulated for all possible driving conditions and are switched with a control strategy. A detailed analysis is done for an idealized system to study the system-level performance, and important modes are identified by creating a histogram analysis for different driving conditions. Various heat pump (HP) waste heat recovery (WHR) configurations are compared against each other and with coolant based positive temperature coefficient (PTC) heaters for different drive cycles, grades, and ambient temperatures. The range increase of the base HP (with no WHR) configuration relative to PTC heating is found to vary from 4-33% with an extra 1-4.4% possible by using idealized WHR. Waste heat recovery is also shown to improve the HP heating capacity by 28%, making its operation feasible at low temperatures. Applicability of the decision tree in the context of various EV TMS designs of leading manufacturers and existing literature is discussed.

To my parents and sisters

TABLE OF CONTENTS

LIST OF FIGURES

LIST OF TABLES

NOMENCLATURE

Acronyms

2P	Two phase
B2C	Battery to chiller
B2Cab	Battery to cabin
COP	Coefficient of performance
D2B	Drivetrain to battery
D2C	Drivetrain to chiller
D2Cab	Drivetrain to cabin
DT	Drivetrain
EV	Electric vehicle
EVTMS	Electric vehicle thermal management system
G	Grade (%)
GIL	General integrated loop
GWP	Global warming potential
HP	Heat pump
HX	Heat exchanger
IC	Internal combustion
LCC	Liquid-cooled condenser
MA	Moist air
PB	Preheated battery
PID	Proportional–integral–derivative
PTC	Positive temperature coefficient
TL	Thermal liquid
TMS	Thermal management system
TXV	Thermostatic expansion valve
UDDS	Urban dynamometer driving schedule
US06	High acceleration aggressive driving schedule
WEG	Water ethylene glycol mixture
WHR	Waste heat recovery
4-W	4-way valve

3-W	3-way valve

Symbols

C	Cooling
C_a	Active cooling
C_p	Passive cooling
C_{whr}	Cooling by waste heat recovery
C_{p+whr}	Passive cooling along with cooling by waste heat recovery
H	Heating
H_a	Active heating
H_p	Passive heating
N	Neutral or isolated, i.e., neither cooling nor heating
T_{amb}	Ambient temperature (°C)
t	Time (seconds)

Subscripts

a	*active*
amb	*ambient*
p	*passive*
p+whr	*passive and waste heat recovery*

1 INTRODUCTION

The rise of electric vehicle (EV) popularity over the last decade for a sustainable future [1,2] demands constant innovation to reach the same or higher levels of performance as well-established internal combustion (IC) engine vehicles [3,4]. Amongst the many recently developed technologies that an EV leverages, its thermal management system (TMS) is sometimes not given enough attention due to its existing presence in traditional IC engine cars [5,6]. However, the thermal architecture for EVs is very different and can drastically affect the overall system performance [7–11]. As opposed to IC engines which generally only require passive cooling using a radiator [12,13], an EV battery has much more stringent thermal requirements [14–17].

Just like a cabin, the EV battery requires both heating and cooling based on the ambient conditions and heat generation [14,18,19]. In mild summers and under normal driving loads, passive cooling is typically sufficient to maintain proper battery operation. However, active cooling using a refrigerant system is often required during aggressive driving conditions, or fast charging [20–22]. The problem worsens in the cold winter months when the battery needs to be warmed to the desired operating temperature for optimal operation of the cells [23,24]. Unlike in an IC engine, the waste heat generated by an EV drivetrain (DT) is much lower and not sufficient to satisfy the heating requirement of both the cabin and the battery [9,25]. This demands an additional heat source which traditionally has been a positive temperature coefficient (PTC) heater. The PTC heater consumes large amounts of energy from the battery and can reduce the driving range of EVs by up to 50% [26–28].

To overcome this range reduction, heat pump (HP) systems for automotive applications have been widely studied [29–33] and can now also be found in production EVs of many manufacturers [34–36]. However, HP technologies face many challenges especially in very cold conditions, typically below 0ºC. Vapor injection techniques can overcome this by improving the HP capacity by 30-70% at low temperatures [37–40]. Another challenge is the accumulation of frost over the outside evaporator heat exchanger (HX) during winter-time heating mode resulting in a loss of HP performance. The frosting-defrosting phenomenon has been investigated for improvements in HP performance by using new fin geometries and hydrophobic surface coatings [41,42]. Heat pump performance can be further improved using ejectors which have been recently studied for automotive applications promising a COP increase of 10-20% [43,44]. Refrigerant selection also plays an important role as it should be optimal for not just cooling performance but

also heating capacity and efficiency. Refrigerant R134a is being gradually phased out due to its higher global warming potential (GWP) and greener alternatives like R1234yf have already been adopted [45]. Other refrigerants like R744 (CO_2) and R32 are also good candidates but have trade-offs and are under active research for usage in EVs [45,46]. All the aforementioned improvements in HP technology are making it a popular alternative to coolant or air-based PTC for EV TMS.

The HP type and integration approach can vary, with different configurations being reported in literature and in real use by commercial EV manufacturers. The commonly used HP configuration generally falls into three categories. Tian et al. [9] demonstrated the applicability of flow reversal across the compressor using a 4-way valve configuration to achieve the HP operating mode. Kiss et al. [47] designed a coolant circuit which can switch coolant line connections to either the chiller and liquid cooled condenser (LCC) of a refrigerant cycle to achieve cooling and heating requirements respectively. This switching of coolant lines using valves for HP operation can also be found in Hyundai-manufactured EVs [34,35]. Use of multiple evaporators and condensers by Tesla is another configuration for HP operation and allows cooling and heating modes by activating and deactivating components differently [36]. Further HP classification can be done based on direct and indirect configuration. The configurations in which heat exchange happens between the refrigerant and air are referred to as direct, whereas the ones which have an intermediate coolant loop between the refrigerant and air are called indirect.

The relatively small amount of waste heat generated in EVs from the drivetrain and battery (once warm enough) can still be used in the EV thermal architecture to boost the EV TMS performance. Different studies have utilized this waste heat for conversion into useful energy to reduce net battery side consumption. Leighton et al. [48] used a combined fluid loop TMS and reported a range improvement of 2% in a HP system by WHR from the power electronics and the electric motor. Tian et al. [9] reported an increase in HP COP by 25% for 1 kW of waste heat generation. The different thermal conditioning requirements of the cabin, battery and drive train components make EV TMS challenging. It is not necessary for the components to require the same kind of conditioning (cooling/heating) at a given time. For example, the battery can require cooling when the cabin requires heating. This requires many thermal modes in an EV TMS to satisfy all the possible combinations of thermal requirements of the components. These modes need to be carefully designed while keeping in mind the architectural constraints of coolant and refrigerant routes and limited number of valves and pumps.

Currently there is a lack in methodologies for early, upfront design space exploration. Such methodologies can enable mapping of trade-offs and identification of optimal TMS design concepts for EVs. Such methods are needed to create thermal system designs with reduced power demand, energy consumption, cost, complexity, and weight while satisfying a range of cooling and heating requirements and system constraints. There is also a need to create enabling elements for an efficient methodology using system modeling and simulation to capture important interactions. Most of the existing literature focuses on one or two aspects of EV TMS. These analyses also generally analyze discrete thermal modes for a given time. However, actual scenarios involve mode switching in real-time and require a control strategy to tackle all possible thermal loads. Hence, it is important to capture the dynamic change in system-level interaction with changing modes and to test various control algorithms. The traditional approach of first designing a thermal architecture and then working around it to satisfy different modes is not well suited for EV TMS as it can lead to design bias and may miss out on potential improvements.

This work overcomes these design and methodology challenges. A decision tree is introduced first for the evaluation of EV TMS design trade-offs concerning system performance. MATLAB-Simulink environment with Simscape is used to develop a simulation framework capable of transient modeling of coolant and refrigerant loops. Using this framework, a general integrated loop is formulated for early upfront evaluation of various configurations and control algorithms for mode switching. Various aspects of WHR are studied in detail to quantify the potential for range improvement in winter conditions. Thermal architecture design is discussed to reflect the applicability of the developed methodology in the context of current designs by leading manufacturers and in the literature. This work outlines a methodology for clean sheet design of EV TMS and develops guidelines to make design decisions with an analysis-driven quantitative approach.

2 MODELING FRAMEWORK

The MATLAB-Simulink Simscape environment is used for modeling, simulation, and analysis of the EV TMS. All relevant model files, simulation results datasets and scripts used in this work are available online on Mendeley Data [49]. The simulation framework can be divided into two parts, first the individual component modeling and then their integration with each other for system-level modeling. The individual components, once developed, serve as the basic building blocks for investigating various system-level configurations and analyzing the overall impact by interchanging thermal loop connections and control algorithms. The Simscape component library is used extensively for representing individual components such as radiators, condensers, evaporators, pumps, compressor, and more. The Simscape language also allows for building custom components with physical connections and equations represented as acausal implicit differential algebraic equations (DAEs).

2.1 Component level Modelling

Every component (Figure 1) has one or more physical domains associated with it in which it operates. For example, single phase thermal liquid, two phase fluid, moist air, thermal, mechanical, and electrical. In the EV TMS, water ethylene glycol (WEG) is commonly used as the coolant and is used in the model for the single-phase thermal liquid domain. For the two-phase refrigerant domain, automotive applications generally use R134a. Since this refrigerant is due to be phased out, the recently adopted greener alternative R1234yf [45] is used in this study. Three kinds of heat exchangers (HX) (Figure 1a) are commonly used in EV TMS and can be categorized based on the two fluids streams: thermal liquid – moist air (TL-MA: radiator, cabin HX), thermal liquid – two phase (TL-2P: chiller, LCC) and two phase – moist air (2P-MA: condenser, evaporator). The cabin is modeled using a constant volume chamber having an air leakage with the ambient. The cabin heat loss to surroundings is dependent on the air leakage, conduction through the walls, glass, roof and convection with the cabin and ambient air. One or more heat exchangers can be connected for heating or cooling the cabin air to maintain the desired setpoint temperature.

The compressor (Figure 1b) is a crucial component of the refrigerant system driving refrigerant flow inside the two-phase domain. It has a proportional-integral-differential (PID) controller for regulating the mass flow rate of the refrigerant in the system based on the thermal conditioning requirements of cabin and battery. Additional constraints such as maximum discharge

pressure, minimum suction pressure and maximum power consumption are also present to ensure the compressor does not cross the operating pressure and power limits. The expansion valve (TXV) having a bulb sensor connected at the compressor inlet is used for the refrigerant expansion (Fig. 1d). The opening fraction of the TXV is decided based on the superheat, subcooling, evaporating and condensing temperatures with the constraint of maximum TXV cooling capacity. A receiver tank is present before the TXV allowing only liquid refrigerant to pass through it (Figure 1d). Importantly, the tank also provides some freedom in the physical system for stable numerical simulations.

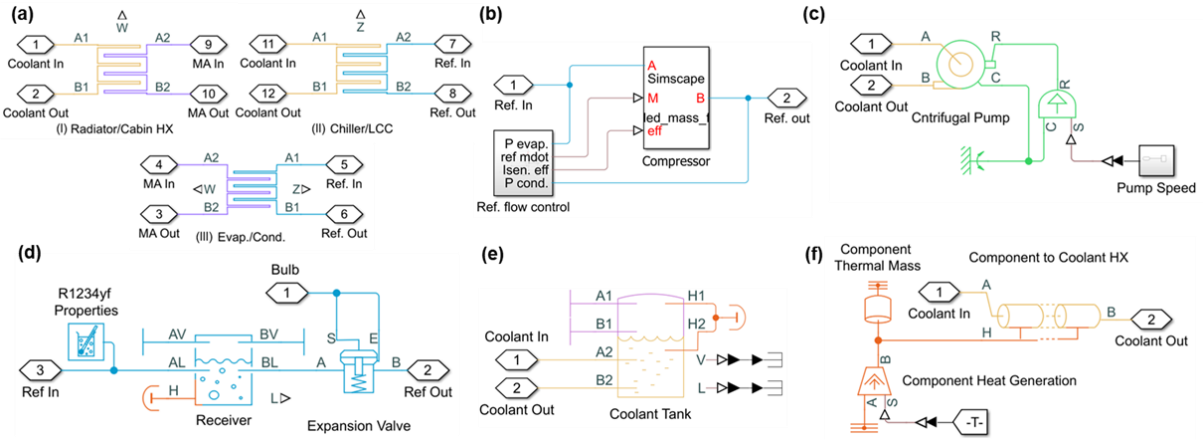

Figure 1. Component-level models used in Simscape. Each color represents a specific fluid circuit or physical domain. Input and output ports are represented by A1, B1 etc. (a) Heat exchangers including thermal liquid-to-moist air (I, radiator or cabin HX), thermal liquid -to-refrigerant (II, chiller or liquid cooled condenser (LCC)), and moist air-to-refrigerant (III, evaporator or condenser). (b) Compressor with a PID based algorithm for refrigerant flow rate control. (c) Centrifugal pump having coolant and mechanical ports with speed as control input. (d) Refrigerant properties, receiver, and expansion valve with an external bulb connection. (e) Thermally insulated coolant tank with insulated thermal and closed gas ports. (f) Heat generating component (such as motor, gearbox, controller, battery) represented with a thermal mass and connected to a coolant circuit for heat exchange.

An EV drivetrain (DT) consists of motors, a motor controller, and a gearbox (Figure 1f). Each component is modeled as a thermal mass with coolant channels for its thermal conditioning. Individual heat loss signals are fed as inputs to generate heat in the thermal masses of the DT components. The battery is modeled in a similar fashion. Although it can be replaced with a more detailed electro-thermal model, it is intentionally kept simple as the focus of this study is to examine the system-level interactions between components. Centrifugal pumps (Figure 1c) are

used to pump fluid through the thermal liquid domain. They are characterized by their pressure drop versus flow rate curves. The pump speed (RPM) can be regulated to control the flow rate. Coolant tanks (Figure 1e) are used in conjunction with pumps to allow the expansion of the thermal liquid and to provide freedom in the physical system for numerical stability, similar to the receiver tank in the refrigerant system. Valves are used extensively to turn on and off the flow of the thermal liquid in the coolant loops and are controlled by signals based on the control algorithm in use. More specific details about each component parameter and models can be found in the online repository [49].

2.2 System-level Integration

The refrigerant system consists of a compressor, TXV and HXs like the chiller, LCC, evaporator and condenser based on the specific configuration being used. These HXs are coupled with either moist air (MA) or thermal liquid (TL) for the active cooling or heating of the cabin and battery. For the EV TMS study herein, the vehicle is modeled to be a four-wheel drive having both front and rear drivetrains. Each drivetrain has a single motor driving the given axle. The motor, motor controller and gearbox are connected in series inside the individual DT thermal loop. The front and rear DT are then connected in parallel to each other. The components are connected to each other either directly or have valves and pumps placed between them for switching thermal liquid flow through the coolant loops. Many systems having different thermal loop architectures can be developed and studied by simply changing the component connections and control algorithms. This is discussed in detail with respect to the general integrated loop (GIL) framework in Section 3.2.

2.3 Drive Cycle and Heat Generation

The battery and DT component heat generation and other relevant signals are obtained from simulating an EV for different drive cycles in the Autonomie software [50]. Autonomie is a vehicle system simulation tool developed by Argonne National Lab. These signals are then fed as an input to the EV TMS model. A midsize passenger EV with a 300 mile all electric range and single fixed gear transmission between the motor and wheels is used for the simulation. Figure 2(a) shows the Autonomie EV model simulation results for a US06 drive cycle in the form of an energy flow diagram. The speed, power and heat generation signals are then processed to make them compatible for being fed as inputs to the EV TMS MATLAB model (Figure 2b, c). Different drive

cycles (US06, UDDS) at different grades (% inclination of road) are simulated to analyze the EV TMS model. The US06 drive cycle is a more aggressive drive cycle than UDDS and has higher power requirements and associated heat losses. The required power and losses also increase with increasing grade for the same drive cycle due to higher torque requirements.

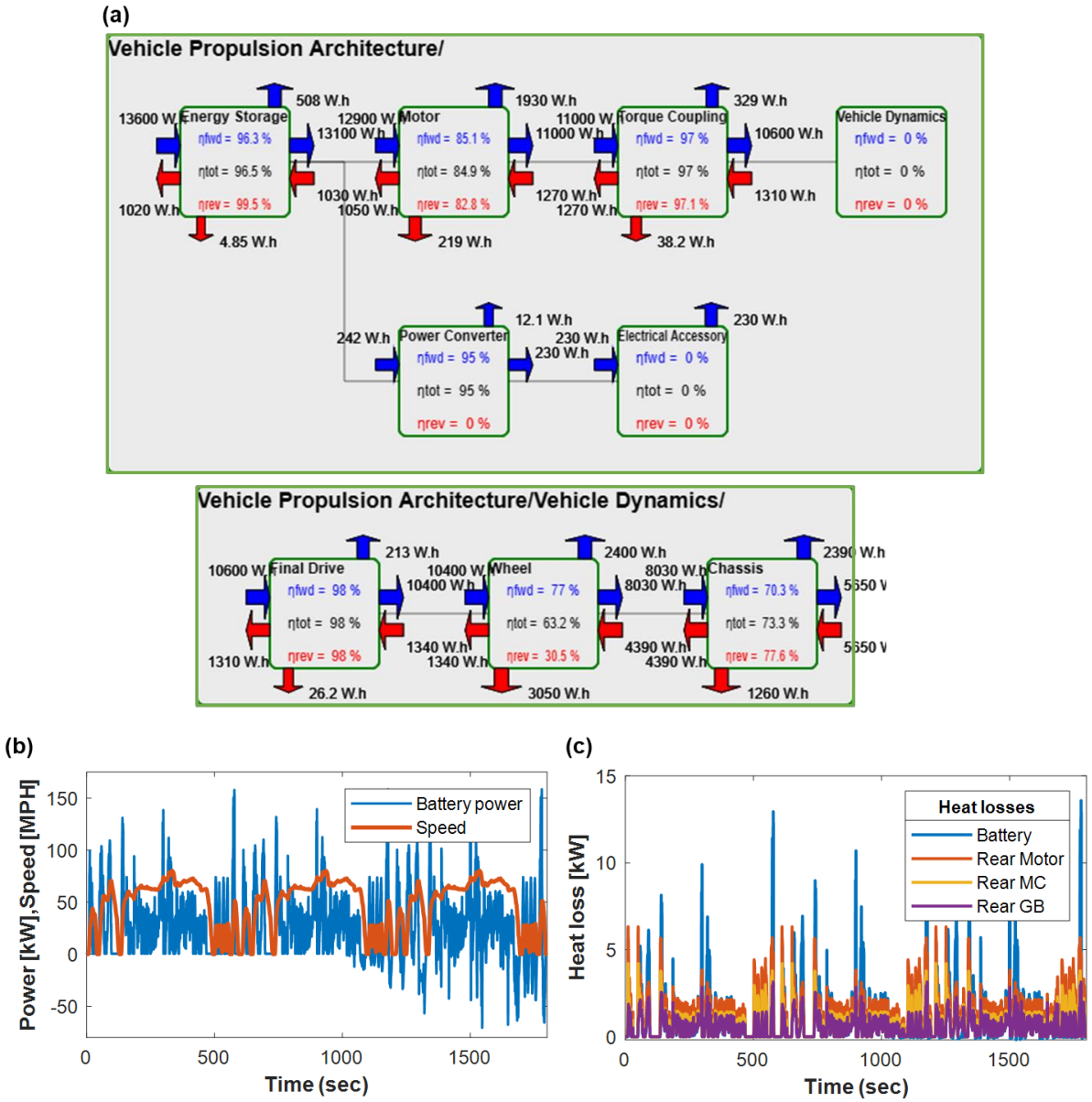

Figure 2. Autonomie EV model simulation results for a US06 drive cycle. (a) Energy flow chart. Blue arrows show forward energy flow required for driving whereas red arrows show reverse energy flow coming from regenerative energy braking. Arrows pointing up or down show heat losses. Numbers inside the block show the forward, reverse, and total energy efficiency (b) Speed and battery power signals as a function of time. (c) Processed heat loss signals of the battery and rear DT (front DT losses are identical).

2.4 Model Tuning and Validation

Parameter tuning and model validation are also performed at two levels: individual component and system-level. These are done for summer cooling scenarios. All experimental data used for validation was obtained from Ford Motor Company. A virtual testbed is modeled in the same Simscape environment for individual analysis of the components. This allows for obtaining component specific results to compare and accordingly tune with the experimental data. Figure 3 shows the experimental and simulated results for component-level validation of the radiator and chiller. The simulated total heat transfer is in good agreement with the experimental data for both components. Initially the increase in heat transfer is significant with increase in air speed (for the radiator) and coolant flow rate (for the chiller) but then becomes marginal with further increase. The simulated pressure drop for the coolant and air are also in close agreement with the experimental data. Note that the simulated coolant pressure drop is relatively linear when compared to the slightly non-linear experimental data. This is acceptable as the radiator and chiller mostly operate inside the region covered in Figure 3 where the deviation is small.

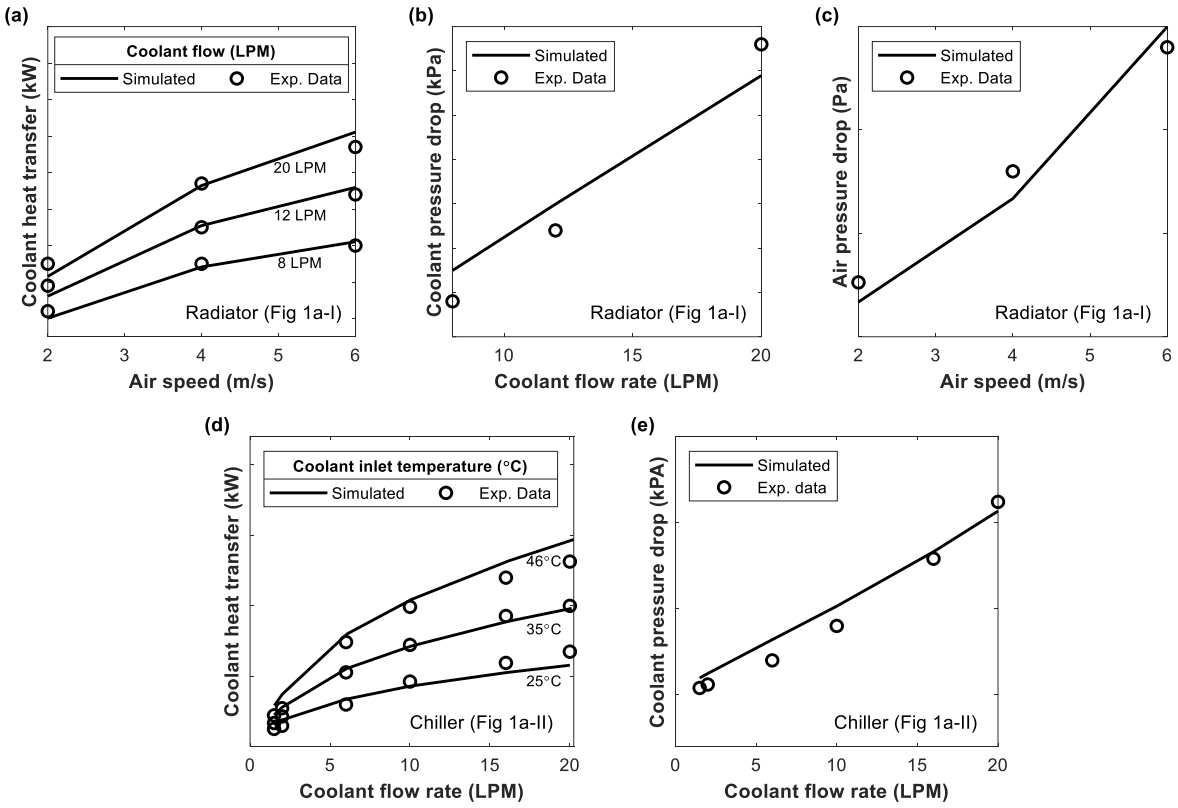

Figure 3. Comparison of experimental and simulated results for radiator (a-c) and chiller (d-e). (a, d) Coolant heat transfer vs flow rate. (b, e) Coolant pressure drop vs flow rate. (c) Air pressure drop vs air speed. Y-axis numerical values removed from the figure due to Ford confidential experimental data.

The system level validations are done by comparing experimental test data of cabin and battery cooling with the simulated results for the same thermal configuration inside the modeling framework. Figure 4 shows the validation results for two summer scenarios, one with only cabin cooling and the other with both cabin and battery cooling at the start followed by only cabin cooling as the battery chiller valve shuts off. The simulated and experimental results show a good match in cabin and battery temperature profiles (Figure 4a, d). The compressor is a critical component for estimating the EV TMS energy requirements which is a key aspect in this work. The simulated compressor results such as power consumption and discharge-suction pressures are compared against test data and show close resemblance (Figure 4b-c, e-f). Cabin evaporator loads are also compared and again relate closely with the experimental data. Note that due to confidential experimental data provided by Ford, the y-axis numerical values are removed from Figure 3 Figure 4 and the specific test conditions and configurations are not disclosed. The component and system-

level validation demonstrate the applicability of the Simscape framework for simulating TMSs. This framework will now be used for analyzing the design methodology for EV TMS.

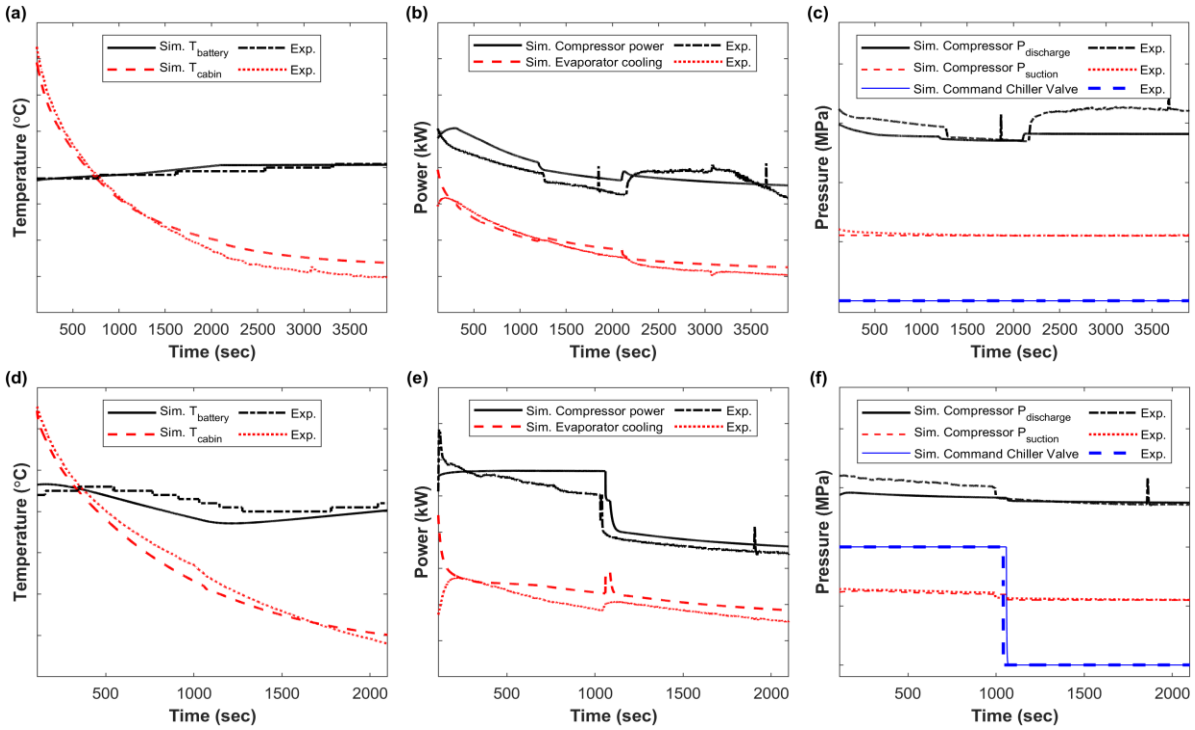

Figure 4. Comparison of experimental and simulated results in summer conditions for (a-c) cabin cooling only, (d-f) both cabin and battery cooling initially followed by cabin cooling only. (a, d) Cabin and battery temperature. (b, e) Compressor power and evaporator cooling. (c, f) Discharge and suction compressor pressure and battery chiller valve command. Y-axis numerical values removed from the figure due to Ford confidential experimental data.

3 METHODOLOGY

3.1 Decision Tree and Trade-offs

Many EV TMS designs are generally experience-based or modified versions of some existing framework. There is currently a lack of efficient methodologies to come up with an optimized clean sheet design for a given set of components. This section formulates a decision tree and quantifies these aspects to allow analysis-driven decision-making for designing a thermal architecture. Figure 5 shows the decision tree representing the guidelines for the EV TMS design. Each level addresses a particular trade-off (marked at T1, T2 etc.) and needs to be analyzed to choose the best option. The EV TMS design should satisfy the thermal requirements of the cabin, battery, and DT, such as desired setpoint and min/max temperature thresholds for different driving and weather conditions, with the target of minimizing TMS energy consumption and design complexity.

The first level (T1) deals with the type of method for conditioning (cooling/heating) the cabin. Traditionally, most vehicles have a direct configuration for cooling purposes employing the simplest layout with compressor, TXV, condenser and evaporator connected in one loop. For heating purposes, generally a coolant loop with a PTC heater is used. However, HPs are becoming popular for EV automotive applications as discussed in Section 0. Figure 6 shows two configurations, direct and indirect, for cabin conditioning utilizing a HP. Both types can cool the cabin in summer and warm it in winter by using a four-way valve for refrigerant flow reversal. The evaporator/condenser (or chiller/LCC in case of indirect) and TXV should have compatibility with interchangeable functionality and bidirectional refrigerant flow for this system to work. For a direct system, the refrigerant rejects or absorbs heat directly from the air (cabin/ambient). The indirect configuration has extra resistance in the form of thermal liquid (coolant) to transfer heat between the refrigerant and air. The refrigerant first exchanges heat with the coolant via TL-2P HX (chiller/LCC, Figure 1a-II) which then exchanges it with the air by using a TL-MA HX (radiator/cabin HX, Figure 1a-I). This extra resistance will lead to higher condensing and lower evaporating temperatures on the compressor side, leading to lower COP. The cooling/heating rate will also be compromised due to added thermal inertia of the coolant. Hence, the direct configuration may seem to be the best due to its expected better performance and design simplicity owing to fewer parts. However, the direct system has disadvantages because of its isolated loop

from the rest of the TMS components. The indirect configuration can be easily interconnected with the other EV TMS systems of the vehicle like the battery and DT with the help of thermal liquid connections and valves. This offers high potential and flexibility for WHR in the winter to maximize energy savings and driving range. Moreover, the indirect configuration allows for the refrigerant system to be packaged closely as one module, saving space and costs by eliminating lengthy refrigerant lines passing throughout the vehicle, which in turn increases HP efficiency and reduces refrigerant charge. The coolant routes coming from the refrigerant module take care of the thermal architecture and are easier to implement when compared to refrigerant lines. For these reasons, the indirect configuration will be studied in this work. However, the performance loss of the indirect configuration with respect to the direct one has been analyzed for determining the cooling/heating rates and is reported in Section 4.1. This information can then be used to appropriately size heat exchangers or the conditioning capacity of the refrigerant system to maintain similar passenger comfort levels for cabin cooling/heating.

The next levels in the decision tree flowchart (T2, T3, Fig. 5) are specifically about heating the cabin and battery for winter conditions. The first choice is to decide between using a traditional and easily implementable PTC heater or a HP system which is much more energy efficient. Section 4.3 quantifies the performance of the two options with respect to energy consumption and effect on driving range. Level T3 states three different configurations via which the HP can be utilized in the EV TMS as discussed briefly in Section 0. Refrigerant flow reversal through the compressor converts a regular AC system to a HP system. Coolant line switching enables HP operation by simply switching the thermal liquid flow in the coolant lines through the LCC and chiller of the refrigerant system based on the thermal conditioning requirements. This requires an indirect system and will be discussed in detail within the GIL framework. Other methods like using multiple evaporators and condensers can also achieve HP operation by activating only one set of components based on the cooling or heating mode. This configuration will be discussed briefly in the layout design Section 4.4.

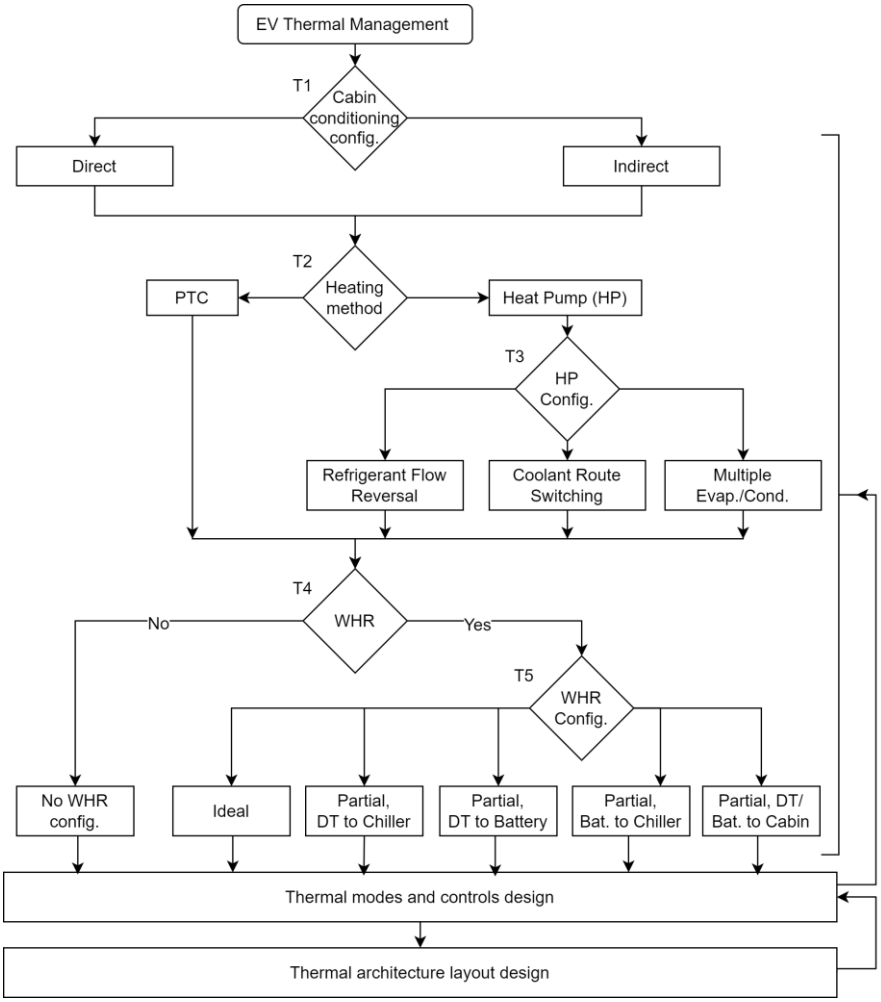

Figure 5. Decision tree flowchart for EV TMS design. Trade-off T1 deals with the selection of the cabin conditioning configuration and T2 deals with the selection of the heating method. Trade-off T3 considers different HP configurations and T4 and T5 considers different WHR configurations. The last two steps pertain to the modes of operation, controls and architecture layout design and can affect the decisions in T1-T5 based on system complexity and practical constraints.

Subsequent levels (T4 and T5) deal with decisions regarding WHR for further range improvements during cold ambient operation. Whether or not WHR is useful is the first decision (T4) and if useful, what type of WHR configuration should be implemented is the next trade-off (T5). The trade-off here refers to a higher system efficiency at the cost of a more expensive and complex EV TMS. T4 and T5 are analyzed using the GIL framework in Section 4.2. The second to last step on modes and controls is discussed in detail in Section 3.4 whereas the last step of the thermal architecture layout design is discussed in Section 4.4 and is intended for future work.

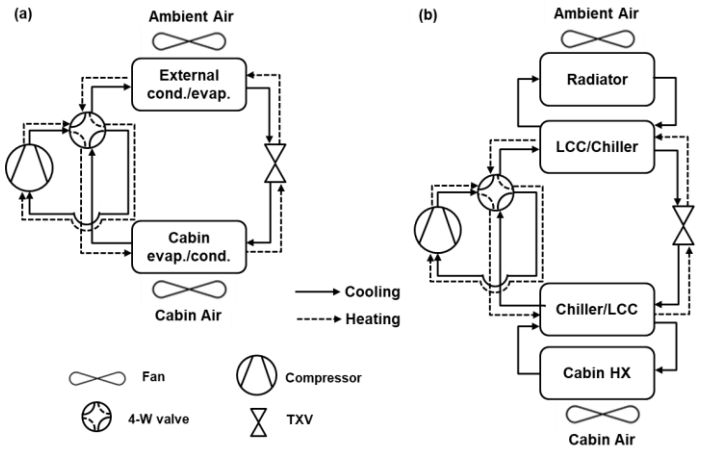

Figure 6. Schematics of EV cabin conditioning configurations showing the (a) direct and (b) indirect layouts. Legend in the bottom left is valid for both schematics. Schematics not to scale.

3.2 General Integrated Loop (GIL)

The GIL (Figure 7) is a framework developed for system-level analysis of different configurations, operating modes, and control algorithms, all in one simulation model using a consistent thermal architecture (model files available online [49]). The GIL acts as a parent configuration from which all other configurations can be tested and analyzed with minimal changes and development time. It is intended to be used as an upfront analysis tool for EV TMS designs to obtain valuable insights without having to invest time to develop prototypes and conduct experiments. The framework utilizes the component models described in Section 2.1 (Figure 1). Following the decision tree (Fig. 5), it is based on using indirect cabin conditioning (T1) and HP for winter (T2) in a coolant route switching configuration (T3). The GIL is then used to evaluate T4, T5 and other remaining aspects of the operating modes. MATLAB-Simulink implementation of the GIL framework using Simscape is shown in Figure 7(b).

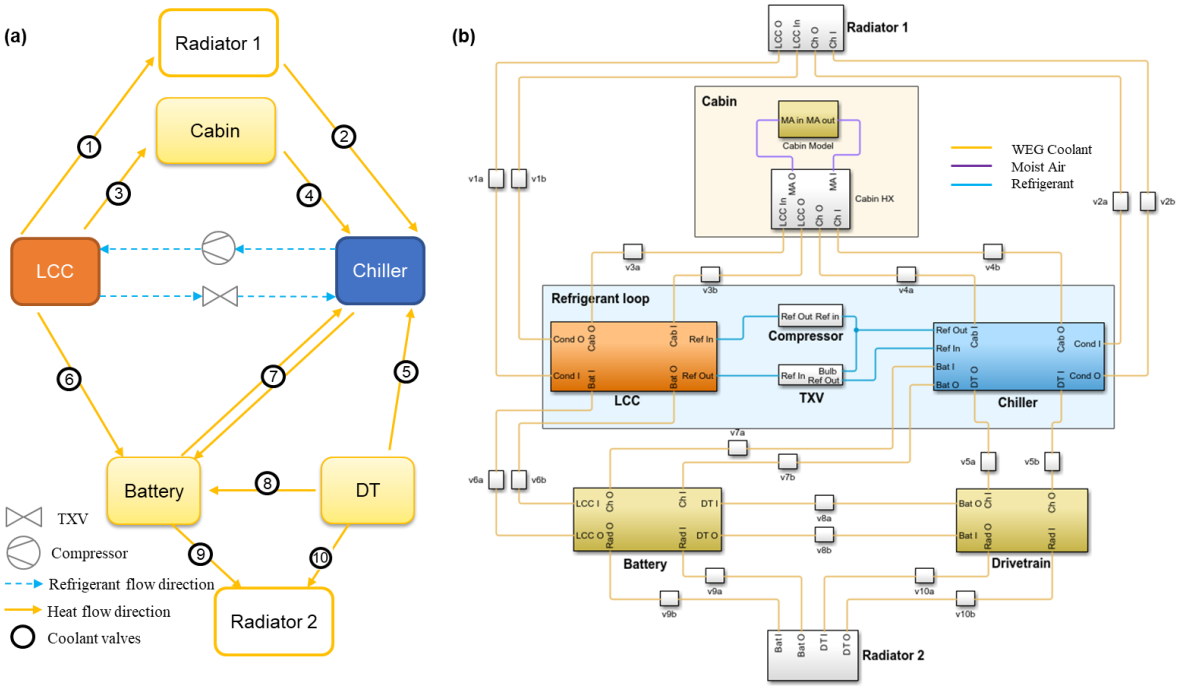

Figure 7. (a) Schematic of the general integrated loop (GIL) showing the EV TMS configuration with refrigerant system at the center. Cabin and Radiator 1 are on top whereas battery, DT and Radiator 2 are on the bottom. Black circles represent coolant valves, while yellow solid lines represent heat flow directions and blue dotted arrows represent refrigerant flow direction. (b) Layout implementation of the GIL framework in MATLAB-Simulink using Simscape. The shaded blue box represents the refrigerant loop.

The circular numbers marked in the GIL schematic (Fig. 7a) represent valves and the solid yellow arrows depict all the possible directions of heat flow associated with the thermal liquid (coolant) flow. The valves can turn on or off the flow of coolant with the intention of connecting or disconnecting one component from the other. The refrigerant loop is situated at the center of the GIL with the chiller and LCC having connections to other components. Cabin and Radiator 1 are shown on top of the schematic whereas the battery, DT, and Radiator 2 are placed at the bottom. The cabin and battery can connect with both the chiller and LCC for active cooling and active heating, respectively. Similarly, Radiator 1 can also be connected to either the chiller or the LCC depending on whether the refrigerant system is working in the heating or cooling mode. The DT and battery can be connected to Radiator 2 for passive cooling. Note that two radiators are used for simplicity and ease of understanding as it allows dedicating one radiator for the refrigerant system (LCC/chiller) and the other for the battery and DT. The DT can also be connected to the battery and chiller for WHR. Similarly, the battery can also give its excess heat to the chiller for

WHR. The connections or the state of valves (on/off) to allow coolant flow between the components is dependent on the operating mode in which the system is running as described in Section 3.4. Each component model has a pump included inside to make sure that there is always at least one pump in any given coolant loop to drive fluid flow.

It is important to note that the application of the GIL is to do a system-level analysis for different coolant connections and control algorithms to determine the most important thermal modes and to evaluate different configurations (e.g., WHR configurations listed in level T5 of the decision tree, Fig. 5). To enable this, the components are allowed to freely interact with one another with the help of simple but numerous on-off valves, pumps, and coolant routes. It is not to be confused with the architecture layout design, which would be restricted by the number of valves (and type like 3/4/5-way), pumps, and complexity of coolant routes that can be afforded in the system. The GIL framework helps in determining which connections and modes would be most important from a system performance point of view assuming no constraints between connecting one component to the other. But these connections need to be analyzed with respect to the system design and complexity as discussed Section 4.4.

3.3 WHR configurations

In the winter, opportunity exists to recover waste heat from the DT and battery for conversion to useful energy. However, there is a lack of studies which exhaustively analyze and compare the contribution of different WHR approaches. This is crucial because the type of WHR configuration affects the cost and complexity of the coolant layout design. The different WHR configurations are described here with the objective of quantifying their relative contribution towards energy savings using the GIL framework. Figure 8 summarizes the individual DT and battery WHR approaches and their combination to give the ideal WHR configuration. The excess heat from the DT can either be given to the chiller or to the battery. The DT-to-chiller (D2C) WHR configuration transfers the heat from the thermal coolant to the refrigerant and increases the suction temperature at the compressor inlet which will lead to higher HP COP. This will be referred to as indirect WHR since the waste heat is not being transferred directly for cabin or battery warmup but is instead being used indirectly to increase system efficiency. The DT can also give its excess heat to a cold battery for passively warming it up to the desired operating temperature (DT-to-battery, D2B WHR). This will be referred to as direct WHR since the DT heat is given directly to the battery via thermal liquid (coolant) flow.

In situations when the battery reaches high temperature due to harsh driving loads or after fast charging, the excess battery heat can be utilized for indirect WHR by giving it to the chiller (battery-to-chiller, B2C WHR) for HP COP increase similar to the D2C configuration. Note that the DT and battery can also be connected to the cabin for DT/battery-to-cabin direct WHR (D2Cab/B2Cab), but this has been omitted from this study for a few reasons. DT heat loads vary significantly with the driving conditions and so will the temperature of the coolant, which will lead to inconsistent heat supply to the cabin and may contribute to passenger discomfort. For the battery, WHR is at relatively low temperatures since the battery high side temperature is generally around 40°C, implying low coolant temperature and very small cabin heating rates. Moreover, keeping the battery and DT separate from the cabin is preferable for keeping the coolant layout less complex. To maximize energy savings all three configurations of WHR need to be present in a system and this is referred to as ideal WHR. The ideal WHR configuration acts as an upper bound for energy savings and can be used as the benchmark to compare with individual WHR configurations. In the no WHR configuration, there is no waste heat recovery of any type, and it can be considered the base case for a HP. The PTC configuration with no WHR is also analyzed to obtain energy consumption and act as a reference for energy savings relative to the HP configurations. All these configurations can be simulated using the GIL framework by only changing the control algorithms and component connections for different operating modes as described Section 3.4.

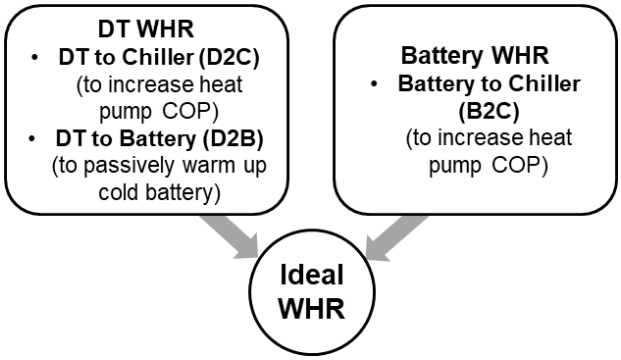

Figure 8. Different waste heat recovery (WHR) configurations.

3.4 Operating Modes

Different operating modes are required for the EV TMS to satisfy the thermal constraints of the cabin, battery, and DT for a wide range of driving and weather conditions. The set of modes also

depends on the WHR capability of the system. Table 1 shows a simplified general list of all modes based on the components and ambient temperature for the ideal WHR configuration. Modes 1-6 are for winter and 7-9 are for summer. Since WHR is most relevant for cold ambient conditions, modes 1-6 will be studied in detail with respect to the available WHR configuration options. The winter sub-modes depend on the WHR configuration, while the summer modes remain the same. In the ideal WHR configuration, all three of the D2B, D2C and B2C WHR capabilities are included, so it has the highest number of modes compared to the individual WHR configurations. For each mode, the control algorithm relates to the GIL framework (Figure 7) by defining the state of its valves. The open valves that allow coolant flow are listed in Table 1, and all other valves remain closed. Since ideal WHR is inclusive of other WHR configurations, its modes will be discussed in detail.

It is important to first discuss the temperature thresholds being used for each component before discussing the modes. For all operating conditions, the cabin requires active thermal management utilizing the refrigerant system to reach the desired set point temperature of 20°C. For the battery and DT, widely used suitable temperature thresholds are chosen [14,19]. In winter conditions, it's assumed that the battery needs warming until it reaches 15°C. Active heating (H_a) is done if the battery temperature is critically low (<5°C) and passive heating (H_p) with D2B WHR (if available, otherwise active heating is continued) is done when the battery temperature is in the range of 5-15°C. This is because if the battery is too cold, it is desired to warm it up as quickly as possible and active heating can provide higher heating capacity in general as compared to D2B WHR. But once the battery temperature is above its critically low temperature, then it can be allowed to warm up using D2B WHR until the desired minimum temperature of 15°C is reached. The battery is put in neutral (N) or isolation once its temperature reaches the 15-25°C range and can be used for B2C WHR if its temperature exceeds 25°C (referred as C_{whr} because the battery WHR cools the battery). If the battery temperature exceeds 40°C, then the radiator is also used for additional cooling along with B2C WHR (C_{whr+p}).

For summer conditions, the battery is put into the passive cooling mode (C_p, i.e., using the radiator) for battery temperature ranges of 25-40°C. When the battery temperature exceeds 40°C, active cooling (C_a, using chiller and the refrigerant system) is done to provide higher cooling capacity. In winters, the drivetrain can either be put in neutral (N) or used for D2C or D2B WHR (C_{whr}) based on its temperature. The D2B or D2C WHR modes are only used if the gearbox

temperature is greater than 25°C because its mechanical efficiency generally reduces significantly at low temperatures. If DT cooling by WHR is not sufficient and the temperature exceeds 90°C, then the radiator is also connected to provide additional passive cooling (C_{whr+p}). For summer conditions, the DT is put in the cooling mode if any of the components (motor, motor controller and gearbox) exceed 50°C.

Mode 1 is a typical cold vehicle start scenario in which both the cabin and battery require active heating. Since the DT is also cold in this mode, it is put in neutral as it does not have enough waste heat to recover. Mode 2 is when the DT becomes warm enough for WHR. There are two options for WHR, either D2B or D2C. As mentioned before, when the battery temperature is critically low, it needs active heating which rules out D2B and leaves D2C to be used (Modes 2a, 2b). The only difference between modes 2a and 2b is that in the case of mode 2b, the DT temperature is very high and so it is being cooled both by WHR and the radiator (the same logic applies to modes 3b, 3d and 6b). If the battery temperature exceeds the critical temperature (>5°C), then D2B is used over D2C (modes 2c, 2d). This is because D2B is a direct WHR configuration (recovering heat directly from DT to battery) compared to indirect B2C WHR (indirectly saving energy by increasing heat pump COP), making it more effective in general as shown later in Section 4.3 when compared to individual WHR energy savings.

In mode 3, both the DT and battery are warm enough to provide waste heat to the chiller. The decision between choosing D2C and B2C is based on whichever has a higher coolant exit temperature amongst the DT and battery. This makes sure that the chiller receives the hotter coolant fluid coming out of the two to maximize WHR. Both D2C and B2C are not used simultaneously as it will lead to mixing of fluid streams between the battery and DT causing unwanted heat transfer from one to the other. In modes 3c, 3d and 4b, following the same logic as for the DT, if the battery temperature exceeds 40°C, then a radiator is connected to provide additional cooling.

Table 1. Different operating thermal modes for the ideal WHR configuration with corresponding valve states in the GIL framework. H- Heating, C- Cooling, N-Neutral/Isolated, a- active, p- passive, whr- waste heat recovery. Empty cells have the same values as the preceding row.

Mode	**T_{amb}** (°C)	**Cabin** (°C)	**Battery** (°C)	**Drivetrain** (°C)	**Open Valves**	**Conditions**
1	<20	H_a	H_a (<15)	N (<25)	2,3,6	Cabin and battery require heating. DT is cold so not available for WHR
2a	<20	H_a	H_a (<5)	C_{whr} (25-90)	3,6,5	Both cabin and battery require heating. DT warm enough for WHR
2b				C_{whr+p} (>90)	3,6,5,10	
2c			H_p (5-15)	C_{whr+p} (25-90)	2,3,8	
2d				C_{whr+p} (>90)	2,3,8,10	
3a	<20	H_a	C_{whr} (25-40)	C_{whr} (25-90)	3,5/7*	Cabin requires heating. Both battery and DT warm enough for WHR (* 5 if $T_{DT\ coolant\ exit} > T_{Battery\ coolant\ exit}$, else 7)
3b				C_{whr+p} (>90)	3,5/7*,10	
3c			C_{whr+p} (>40)	C_{whr} (25-90)	3,9,5/7*	
3d				C_{whr+p} (>90)	3,9,5/7*,10	
4a	<20	H_a	C_{whr} (25-40)	N (<25)	3,7	Cabin requires heating. Only battery is warm enough for WHR
4b			C_{whr+p} (>40)		3,7,9	
5	<20	H_a	N (15-25)	N (<25)	2,3	Cabin requires heating. Both battery and DT not warm enough for WHR
6a	<20	H_a	N (15-25)	C_{whr} (>25)	3,5	Cabin requires heating. Only DT is warm enough for WHR
6b				C_{whr+p} (>90)	3,5,10	
7a	>20	C_a	C_p (25-40)	C_p (>50)	1,4,9,10	All three require cooling
7b			C_a (>40)		1,4,7,10	
8a	>20	C_a	C_p (25-40)	N (<50)	1,4,9	Only cabin and battery require cooling
8b			C_a (>40)		1,4,7	
9a	>20	C_a	N (<25)	N (<50)	1,4	Only cabin requires cooling
9b				C_p (>50)	1,4,10	

In mode 4, the battery is warmed up and the DT is not. Hence, B2C WHR is used. In mode 5, both battery and DT are in neutral states and do not contribute towards any WHR. In mode 6, the battery temperature is such that neither heating or cooling is required (a neutral state) and the DT is warm enough for D2C WHR. The rest of the modes are for summer conditions in which the cabin, battery and DT may require cooling based on their temperatures. In 7a and 8a the battery is cooled passively whereas in 7b and 8b it is cooled actively. The DT is either in neutral state (7a, 7b) or in the passive cooling mode (8a, 8b). Note that the DT is never cooled actively as it will waste compressor energy and the maximum DT temperature threshold is high enough for passive cooling to be sufficient. The battery requires active cooling because it has relatively low maximum operating temperature. Both the battery and DT are in the neutral state in mode 9a whereas in mode 9b, the battery is in neutral while the DT requires cooling. The control algorithm checks the component temperatures at every step to select an operating mode for the system.

Table 2 shows the winter modes for the individual WHR configurations (i.e., when the system can do only one type of WHR). The general idea for defining the modes is the same as that of the ideal WHR table (Table 1). The configuration not using any WHR has the least modes and is the simplest. Sub-modes are added to the no-WHR modes to define the modes for the D2C, D2B and B2C WHR configurations capable of doing their respective type of WHR. The ideal WHR configuration discussed in Table 1 can be considered as a union of all these individual WHR capabilities.

Table 2. Modes for different WHR configurations, including the (a) No WHR configuration, (b) D2C WHR configuration, (c) D2B WHR configuration, and (d) B2C WHR configuration. H- Heating, C- Cooling, N-Neutral/Isolated, a- active, p- passive, whr- waste heat recovery. Empty cells have the same values as the preceding row.

(a) No WHR

Mode	T_{amb} (°C)	Cabin (°C)	Battery (°C)	Drivetrain (°C)	Open Valves
1	<20	H_a	H_a (<15)	N (<50)	2,3,6
2	<20	H_a	H_a (<15)	C_p (>50)	2,3,6,10
3	<20	H_a	N (15-25)	N (<50)	2,3
4	<20	H_a	N (15-25)	C_p (>50)	2,3,10
5	<20	H_a	C_p (>25)	N (<50)	2,3,9
6	<20	H_a	C_p (>25)	C_p (>50)	2,3,9,10

(b) DT to Chiller WHR

Mode	T_{amb} (°C)	Cabin (°C)	Battery (°C)	Drivetrain (°C)	Open Valves
1	<20	H_a	H_a (<15)	N (<25)	2,3,6
2a	<20	H_a	H_a (<15)	C_{whr} (25-90)	3,6,5
2b				C_{whr+p} (>90)	3,6,5,10
3	<20	H_a	N (15-25)	N (<25)	2,3
4a	<20	H_a	N (15-25)	C_{whr} (25-90)	3,5
4b				C_{whr+p} (>90)	3,5,10
5	<20	H_a	C_p (>25)	N (<25)	2,3,9
6a	<20	H_a	C_p (>25)	C_{whr} (25-90)	3,9,5
6b				C_{whr+p} (>90)	3,9,5,10

(c) DT to Battery WHR

Mode	T_{amb} (°C)	Cabin (°C)	Battery (°C)	Drivetrain (°C)	Open Valves
1	<20	H_a	H_a (<15)	N (<25)	2,3,6
2a	<20	H_a	H_a (<5)	C_p (>25)	2,3,6,10
2b			H_p (5-15)	C_{whr} (25-90)	2,3,8
2c				C_{whr+p} (>90)	2,3,8,10
3	<20	H_a	N (15-25)	N (<50)	2,3
4	<20	H_a	N (15-25)	C_p (>50)	2,3,10
5	<20	H_a	C_p (>25)	N (<50)	2,3,9
6	<20	H_a	C_p (>25)	C_p (>50)	2,3,9,10

(d) Battery to Chiller WHR

Mode	T_{amb} (°C)	Cabin (°C)	Battery (°C)	Drivetrain (°C)	Open Valves
1	<20	H_a	H_a (<15)	N (<50)	2,3,6
2	<20	H_a	H_a (<15)	C_p (>50)	2,3,6,10
3	<20	H_a	N (15-25)	N (<50)	2,3
4	<20	H_a	N (15-25)	C_p (>50)	2,3,10
5a	<20	H_a	C_{whr} (>25)	N (<50)	3,7
5b			C_{whr+p} (>40)		3,7,9
6a	<20	H_a	C_{whr} (>25)	C_p (>50)	3,7,10
6b			C_{whr+p} (>40)		3,7,9,10

4 RESULTS AND DISCUSSION

4.1 Direct versus Indirect Conditioning

The direct and indirect configurations, as discussed in Section 3.1 are analyzed for cooling and heating performance. Figure 9(a, b) show the results for cabin temperature in the heating and cooling modes at 0°C and 35°C, respectively. The indirect configuration takes 5.3 and 6.5 min (1.64 and 1.66x) longer than the direct configuration for heating and cooling, respectively, due to the added thermal resistance and inertia of the coolant loop in between the refrigerant and moist air. The two configurations are further analyzed at different ambient conditions in Figure 9(c, d) for conditioning time and COP, respectively. Time to reach the desired setpoint increases for both configurations as the ambient temperature becomes colder or hotter due to higher cabin conditioning loads. Indirect conditioning is always slower and takes 1.6 to 1.8x longer when compared to direct conditioning for varying ambient conditions. For both configurations, the COP decreases as the ambient temperature increases for both cooling and heating modes. This is expected since the HP efficiency decreases with lower evaporating or higher condensing temperatures. The indirect configuration has a lower efficiency with COP ranging from 18-31% and 31-41% lower when compared to direct configurations for heating and cooling, respectively. It is interesting to note that the relative decrease in COP at hotter or colder conditions for the direct system is more than that of the indirect system. This is because for the indirect system, the effect of ambient temperature acts over an existing resistance of the thermal liquid, leading to a lower relative effect when compared to a direct system which is more sensitive to ambient temperature since it exchanges heat with it directly. Despite its drawbacks, the indirect system is becoming popular for EV TMS because it offers higher flexibility in designing the thermal architecture, as discussed in Section 3.1. The performance loss of the indirect system can be minimized by appropriately sizing the components for meeting similar performance requirements as that of a direct system.

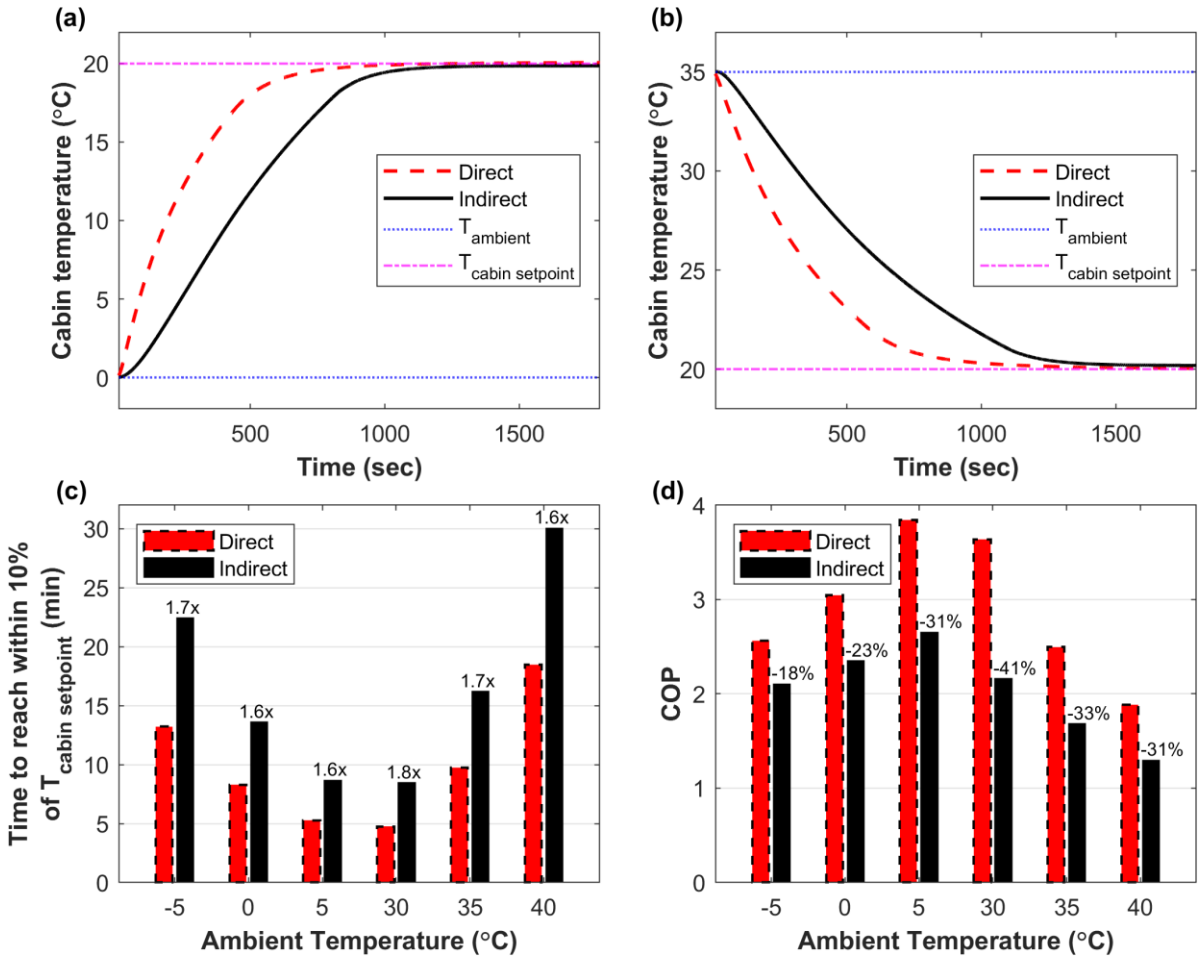

Figure 9. Performance comparison of direct and indirect conditioning configuration for (a) cabin heating (T_{amb} = 0°C), (b) cabin cooling (T_{amb} = 35°C). (c) Time required to reach within 10% of the cabin set point temperature as a function of ambient temperature. The number on top of the bars indicates the factor by which indirect conditioning time is longer relative to the direct conditioning time. (d) COP as a function of ambient temperature. The number on top of the bars indicates the % COP loss for the indirect system relative to the direct system.

4.2 General Integrated Loop (GIL) and Operating Mode

The results of the GIL framework for the ideal WHR mode configuration (Table 1) are all plotted together in Figure 10 for easier understanding of different interactions and their effect and dependency on each other. The ambient temperature is 0°C which is also taken as the initial temperature of the cabin, battery (i.e., no preheating) and DT components to represent a cold start scenario. The simulated drive cycle is a US06 (grade 0) which is repeated 3 times totaling 38.6 km of driving within 30 mins. The current mode state (Figure 10a) of the system is set by the control algorithm based on the temperature of the cabin, battery, and DT (Figure 10b) according to the

mode selection criteria listed in Table 1. The compressor, pump power, and energy consumption are shown in Figure 10(c). Figure 10(d) shows the coolant flow rates through the components. Figure 10(e, f) and Figure 10(g, h) track the heat flow rates and coolant temperatures respectively across the different components.

The system starts from mode 1 (Table 1) as both cabin and battery require heating, and the DT is not warm enough to provide any WHR. The compressor is set to operate in the refrigerant loop to provide the required heating load through the LCC. Since the LCC heat load requirements are high at the start, the compressor tries to work at its maximum power of 4kW (Figure 10c). The actual values are slightly lower because the compressor also needs to satisfy other constraints of maximum discharge and minimum suction pressure thresholds. Since the cabin and battery are connected in parallel to the LCC, the coolant flow rates add up when passing through the LCC (Figure 10d). Similarly, the coolant exit temperature at the LCC is equal to the coolant inlet temperature at the cabin and battery. The coolant exit temperature at the cabin and battery drops as it rejects heat, followed by a rise as it passes through LCC to absorb heat (Figure 10(g ,h)). This active heating by the LCC causes the battery and cabin temperature to rise (Figure 10b). Note that in addition to active heating, the analysis also includes battery internal heat generation which also contributes towards its temperature rise. The chiller flow rate is the same as radiator 1 as they are connected in the same loop. The chiller absorbs heat from the coolant, dropping its temperature below the ambient. The cold coolant then absorbs heat from the ambient as it passes through radiator 1, leading to a rise in coolant temperature at the exit. The DT components, which are left isolated in mode 1 with no coolant flow, also warm up in the analysis due to their own heat losses.

As soon as the gearbox goes above the minimum temperature threshold of 25°C for WHR, the system switches to mode 2a (Table 1) at $t \approx 250$s (Figure 10a). The battery is still in active heating mode because its temperature is still lower than the critical threshold of 5°C. The chiller is disconnected from radiator 1 and connected to the DT to utilize D2C WHR. Immediately after switching to mode 2a, a large amount of heat flows from the DT to the chiller due to a high-temperature difference between the two components. This can be seen as a peak in DT and chiller heat flows (Figure 10(e, f)). The rise in the chiller coolant inlet temperature due to the flow of relatively hot coolant from the DT should lead to an increase in the evaporator temperature of the heat pump, benefiting its COP. The use of D2C WHR also benefits the LCC as its heating capacity increases with only a slight increase in compressor power, confirming the COP increase. Due to

the large amount of heat exchange in a short time, the DT temperature drops quickly and the model switches back to mode 1 when the gearbox temperature goes lower than 15°C (Figure 10b, hysteresis is kept as 10°C, i.e., DT WHR gets activated at 25°C and deactivates at 15°C). The system then stays in mode 1a until the gearbox becomes warm again, switches to mode 2a ($t \approx$ 375s) and comes back to mode 1a. At $t \approx$ 500s the system now switches to mode 2c instead of 2b. This is because the battery is past the critical temperature of 5°C (Figure 10b) and can now be passively warmed up using D2B WHR. The coolant flow rate thus becomes the same for DT and battery. Mode 2c leads to an increase in cabin heating rate as LCC does not have to heat the battery actively. This can be seen as an increase in the slope of the cabin temperature profile (Figure 10b) caused by the rise of coolant inlet temperature in cabin HX (Figure 10h) leading to more heat flow. The compressor power drops to zero (Figure 10c) as the cabin temperature reaches the desired temperature setpoint of 20°C at $t \approx$ 750s while the system continues to run in mode 2c. When the battery reaches 15°C at $t \approx$ 1000s, the system switches to mode 6a, and the battery is put in neutral as it no longer requires passive D2B WHR warmup. The battery coolant flow rate drops to zero, whereas the chiller flow rate matches the DT coolant flow rate since they are now connected for D2C WHR. This leads to a temperature drop of the DT components similar to that which occurred in mode 2a. The system continues to run in mode 6a for the rest of the cycle, with the battery temperature rising slowly due to its own heat generation. The compressor occasionally turns on to maintain the cabin temperature close to the set point of 20°C by a PID-controlled flow rate of refrigerant. This implies lower LCC and chiller heat loads leading to a reduction in cooling of DT components by D2C WHR, causing the temperature of the motor, gearbox, and controller to rise steadily (Figure 10b) . If the cycle were to continue eventually the DT temperature will cross its maximum threshold of 90°C forcing the system to switch to mode 6b. In mode 6b, a radiator will be connected to the DT for passive cooling in addition to D2C cooling, which wouldn’t provide enough cooling on its own due to lower chiller loads.

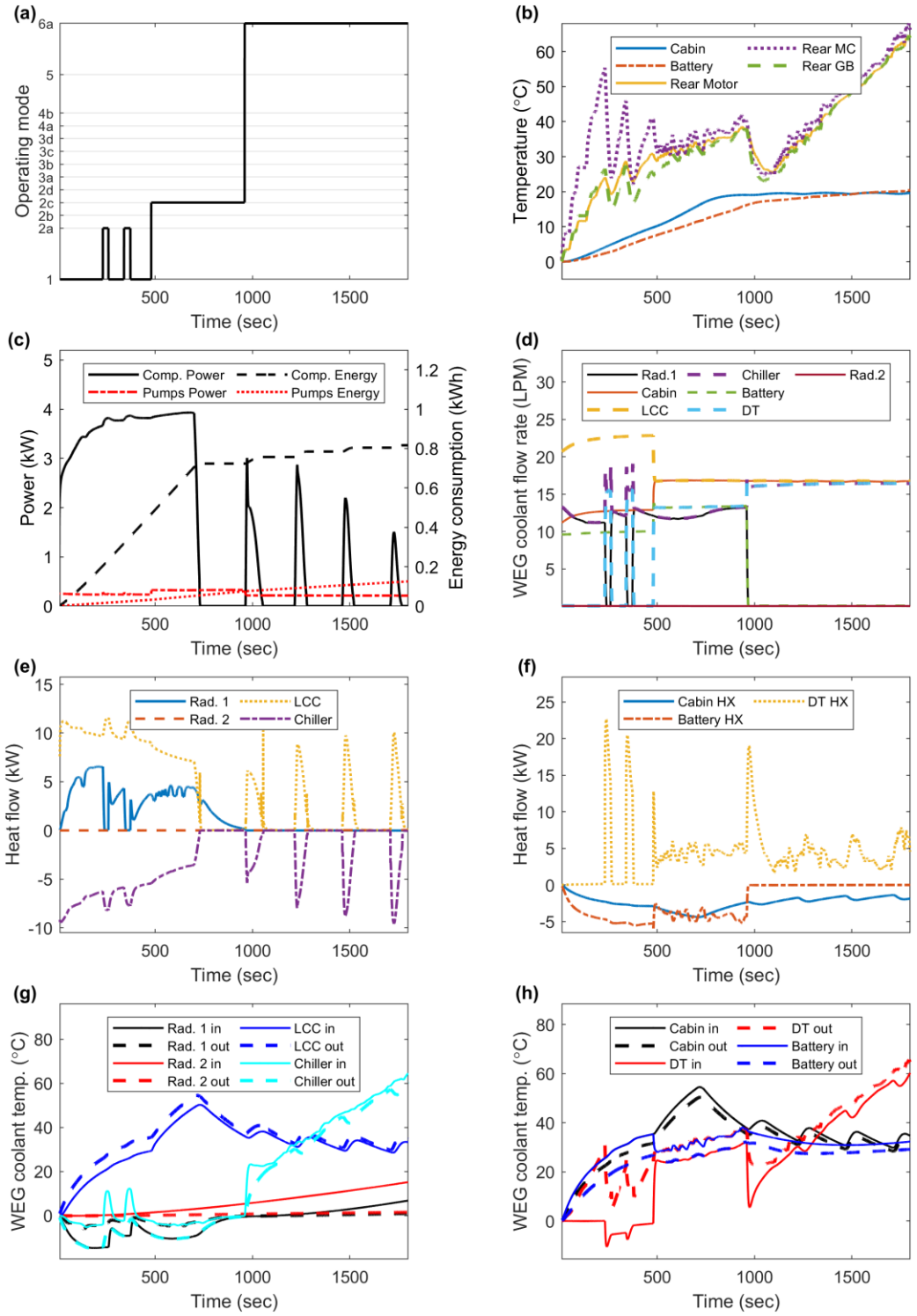

Figure 10. GIL analysis results as a function of time for US06 drive cycle (zero grade, repeated 3 times) at T_{amb}=0°C for ideal WHR configuration. (a) Operating mode switching based on the thermal state of the system as listed in Table 1. (b) Temperature profiles of cabin, battery, and DT components. (c) Power and energy consumption of the compressor and pumps. (d) WEG coolant flow rates through components. (e, f) Heat flow rate through components. (g, h) Coolant inlet and exit temperatures across components.

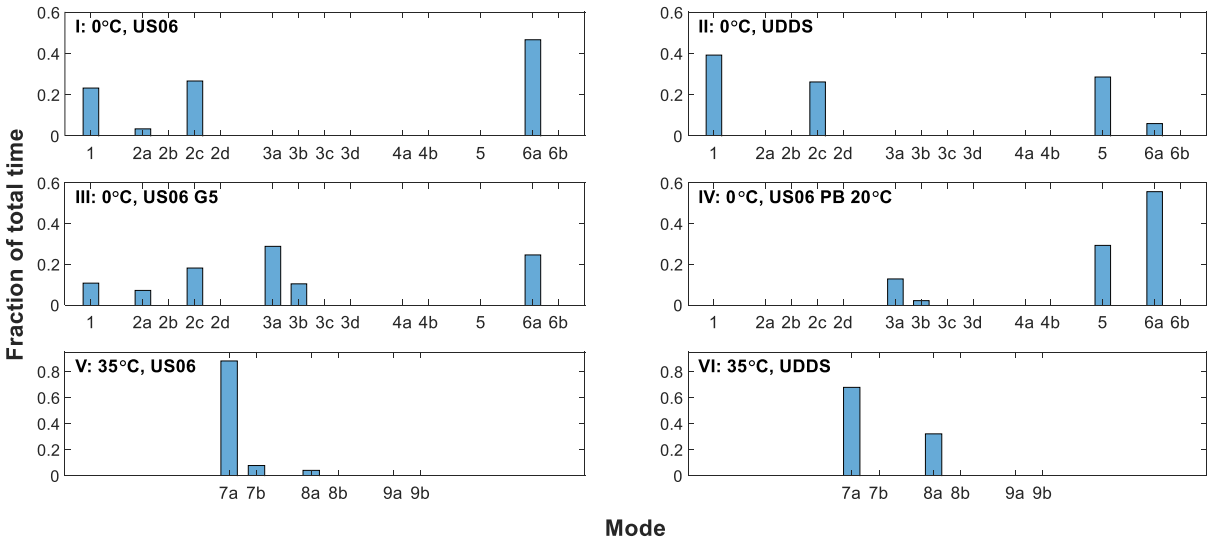

Figure 11. Mode histogram for different ambient temperatures, drive cycles, grades, and battery preheat states (PB – preheated battery, G- grade). The first term in the legend represents the ambient temperature, while the second term represents the drive cycle. By default, the drive cycle grade is zero and battery is not preheated unless stated otherwise. Cases I-IV are for cold conditions and Cases V-VI are for summer conditions.

A histogram can be generated from mode versus time data to evaluate the relative time fraction the system stays in a particular mode. This helps to determine the critical modes which are in operation most of the time. Since a mode reflects a particular arrangement between components, knowing critical modes is equivalent to knowing the set of functionalities and connections which are important for a system to operate efficiently. This becomes very useful when designing thermal loop architectures where only a limited number of functionalities and connections can be implemented due to complexity constraints. Figure 11 shows the histogram for the default case discussed in Figure 10 along with various other driving conditions such as drive cycle, grade, ambient and battery initial temperature. For the default scenario (case I) at 0°C ambient and US06 drive cycle, mode 6a has the highest occurrence followed by modes 1, 2c and a small fraction of 2a. Case II has the same conditions but a different drive cycle (UDDS), which is less aggressive, consumes less energy and thus has lower waste heat generation by the battery and DT. This means that the battery will take longer to heat, which is reflected by an increase in the mode 1 time fraction. The DT also will not have enough heat generation leading to an absence of mode 2a, a reduction in mode 6a and an increase in mode 5. Case III has the same US06 drive cycle as case I but with a grade of 5, which increases energy consumption and heat generation.

Hence, the battery heats up quickly, as seen by a smaller mode 1 and 2c fraction. The mode 2a time fraction is slightly increased due to the higher available DT WHR. Modes 3a and 3b also come into operation, implying that both the DT and battery got hot enough to act as a waste heat sources. Case IV is for a preheated battery to 20°C, all other things being the same as in case I. Since there is no need to heat the battery, modes 1 and 2 are absent. The system mostly stays in modes 6a and 5, switching between D2C WHR activation and deactivation. The slight occurrence of modes 3a and 3b again implies that the battery was preheated to 20°C, and reached the threshold of 25°C to offer waste heat. Summer weather results at 35°C ambient are shown in cases V and VI for the US06 and UDDS cycles, respectively. The UDDS cycle uses passive cooling of the battery (mode 8a) and battery and DT combined (mode 7a). The US06 drive cycle, being more aggressive, requires some occurrence of mode 7b to achieve active cooling of the battery due to higher heat generation.

4.3 Assessment of WHR Configurations

The EV TMS energy consumption and cabin and battery temperature profiles for the different WHR configurations discussed in Section 3.3 are shown in Figure 12. The driving conditions are the same as for the GIL analysis of ideal WHR in Figure 10. The energy consumed and temperature profiles are the same for all configurations until $t \approx 600$s. Due to cold start, the DT and battery cannot be used for WHR until they are warm enough. Table 3 summarizes the TMS energy (compressor and pump) consumption, energy savings and range increase for different WHR configurations along with the PTC heating method as reference. The increase in EV range is calculated using Equation (1) to analyze the system-level impact of TMS energy savings. The energy per kilometer consumption for the US06 drive cycle (grade 0, repeated three times) is 302.6 Wh/km for a total distance of 38.6 km as calculated from Autonomie simulation results (Section 2.3).

$$\%\ Range\ Increase = \frac{\text{TMS energy savings [Wh]}}{\text{Energy per km } \left[\frac{\text{Wh}}{\text{km}}\right] \text{ x Total distance [km]}} \text{x } 100 \qquad (1)$$

The base version utilizing a HP with no WHR performs better than the PTC version. A TMS energy savings of 52.1% and range increase of 12% is observed. The performance further improves when the HP is coupled with WHR. Amongst different HP WHR configurations, ideal

WHR gives the highest TMS energy savings of 12.9% equivalent to an extra range increase of 2.9% over the base HP configuration as it can utilize all the three individual WHR methods. No WHR and B2C have the same performance throughout because the battery could never reach the temperature threshold of 25°C to act as a WHR source. The D2B version has an extra range improvement of 1.7% over the HP base and performs slightly better than the 1.2% increase of D2C. This is expected because D2B enables direct WHR and delivers useful heat straight to the battery for warmup. The D2C design saves energy indirectly by increasing HP COP.

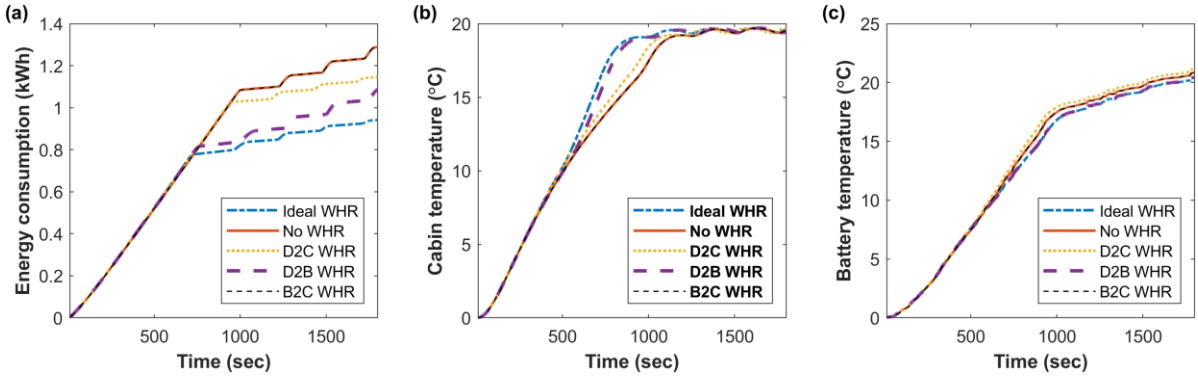

Figure 12. Comparison of system performance for different HP WHR configurations including ideal, D2C, D2B, B2C and no WHR (T_{amb} = 0°C, US06 drive cycle with zero grade repeated three times). The figure shows the time variation of (a) energy consumption of the EV TMS by the compressor and pump, (b) cabin temperature and (c) battery temperature. The B2C and no WHR configuration have overlapping graphs.

It is important to study the breakdown of compressor energy consumption into two parts. The first 15 mins when the heat load requirements are very high to bring the cabin and battery to the desired setpoint. Then the subsequent 15 mins in which a relatively small amount of cabin heating is required to compensate for continuous heat loss to the surroundings to maintain the desired setpoint temperature. Note that the battery only needs to be heated once because losses to surroundings are assumed to be negligible so its own heat generation will keep increasing its temperature afterward. The D2B WHR design saves more energy in the first half by saving on the initial heating energy requirement of the battery and does not have much effect in the second half. On the other hand, the D2C design does not provide an advantage in the first half but saves energy in the second half once the DT temperature reaches relatively high values for better utilization of waste heat to increase COP of the HP. The ideal WHR design uses both D2B and D2C and thus saves energy throughout the run. The ideal WHR design is also the quickest to heat the cabin, with

a 30.1% higher heating rate compared to the no WHR design. This is followed by D2B (24.7%), which is higher than D2C (5.6%) as D2B relieves the load on the LCC, causing an increase in cabin heating. The battery heating rate (with respect to no WHR) for the ideal and D2B designs are slightly lower (-4.6%, -4.5%) because of slower passive warmup of the battery relative to active heating by the LCC in other configurations, amongst which D2C is the fastest (3.5%) due to the LCC capacity increase.

Table 3. Energy consumption and savings for the PTC and different HP WHR configurations. D2C – drivetrain-to-chiller, D2B – drivetrain-to-battery, B2C – battery-to-chiller, HP – heat pump, PTC – positive temperature coefficient, TMS – thermal management system.

Heating Method	**WHR Config.**	**TMS Energy [Wh]** *(Compressor/PTC + Pump)*		**Total [Wh]**	**TMS Energy savings [%]**	**Range Increase [%]**
		0-15 min	15-30 min	0-30 min	With respect to PTC + No WHR *(Increase with respect to base HP + No WHR)*	
PTC	**No WHR**	2036 *(1995+41)*	652 *(615+37)*	2688	-	-
HP	**No WHR** (HP Base)	973 *(909+64)*	315 *(250+65)*	1288	**52.1**	**12.0**
HP	**Ideal**	794 *(724+70)*	147 *(92+55)*	941	**65.0** *(+12.9)*	**14.9** *(+2.9)*
HP	**D2C**	980 *(920+60)*	166 *(113+53)*	1146	**57.4** *(+5.3)*	**13.2** *(+1.2)*
HP	**D2B**	829 *(757+72)*	258 *(192+66)*	1087	**59.6** *(+7.5)*	**13.7** *(+1.7)*
HP	**B2C**	973 *(909+64)*	315 *(250+65)*	1288	**52.1** *(+0.0)*	**12.0** *(+0.0)*

As discussed in Section 0, it is well known that the HP struggles to operate efficiently at low ambient temperatures due to reduced heating capacity. Figure 13 shows the LCC heating capacity and cabin and battery temperature profiles for ideal and no WHR configuration with the same driving conditions as before except a lower ambient temperature of -10°C. As expected, the regular HP system with no WHR fails to deliver enough heat to warm the cabin and battery to their desired setpoint temperatures within the simulated cycle time of 30 mins. However, the ideal WHR configuration increases the LCC heat load by 28.4% due to heat recovery from the DT leading to peaks and drops corresponding to D2C WHR activation and deactivation (Fig. 13a). Note that the drop in LCC heat capacity at the end in the case of ideal WHR is intentional due to the cabin almost reaching the desired set point of 20°C and the battery heating switching from active to passive after crossing the critical threshold of 5°C. Other WHR configurations of D2B and D2C will have

heating rates in between the ideal and no WHR results. The B2C design will be the same as the no WHR design because the battery will not be warm enough to act as a heat source. From this analysis, it can be concluded that WHR not only helps in energy savings but also makes the HP feasible at low ambient temperature by increasing the heating capacity.

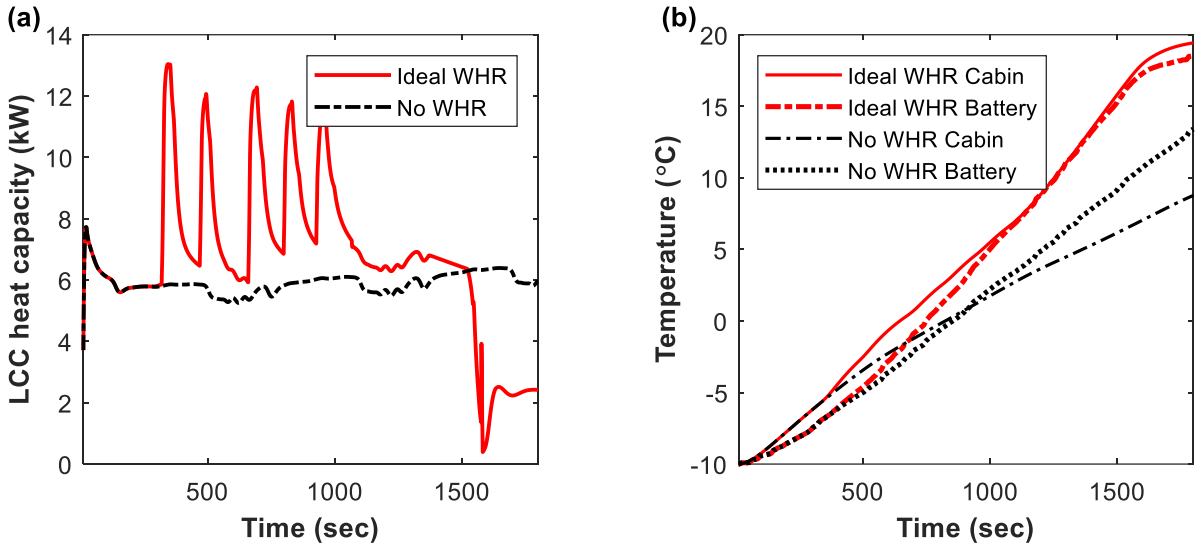

Figure 13. Heat pump performance comparison for the ideal WHR (red lines) and no WHR (black lines) configurations at T_{amb} = -10°C (US06 drive cycle) as a function of time for (a) LCC heat capacity, and (b) cabin and battery temperature profiles.

The TMS energy consumption is compared for ideal and no WHR configuration for different drive cycles & grades (Figure 14a) and ambient temperature & battery preheat state (Figure 14b). TMS energy consumption (for both ideal and no WHR) reduces for a more aggressive drive cycle (US06 vs UDDS) and higher grades (grade 5 vs 0). This is because aggressive driving conditions cause higher battery self-heat generation reducing the requirement of external heating and thus TMS energy. Energy savings (energy difference between ideal and no WHR configuration) depend on two factors, the amount of waste heat generated and battery heating requirement. Energy savings should increase with higher waste heat but only if there is enough requirement for its potential use. In the case of US06 cycle with a grade of 5, the waste heat increases but the battery's self-heat generation reduces the external heating requirement leading to a lower potential for utilizing WHR and thus slightly lower savings. However, that's not the case with UDDS drive cycle and there is still enough potential for waste heat utilization as seen by the increase in energy savings with increasing grade. The system-level impact of TMS

energy consumption and savings on range increase relative to PTC no WHR configuration is shown as numbers on top of the bar graphs in Figure 14. The increase in range by 33.4% for HP no WHR configuration in UDDS cycle is very prominent and shows that even the base HP configuration can give huge advantage for regular urban city driving conditions. The increase is even higher for HP with ideal WHR adding an extra 4.4% resulting in a 37.8% range increase. The much higher range increase of HP configurations for UDDS as compared to US06 can be deduced from equation 1. UDDS cycle has a much shorter travel distance than US06 for the same time period (17.5 vs 38.6 km) and consumes less energy per km (268.4 vs 302.6 Wh/km). In terms of physical interpretation this implies that for UDDS cycle the amount of energy spent on driving for a given time duration is much less than US06, and thus the energy spent on TMS is a larger fraction of the total energy being consumed from the battery. Therefore, any savings on TMS energy will have a relatively high impact on the driving range. For similar reasons, the range increase is lower at higher grades of drive cycles because of a significant increase in energy consumed per km.

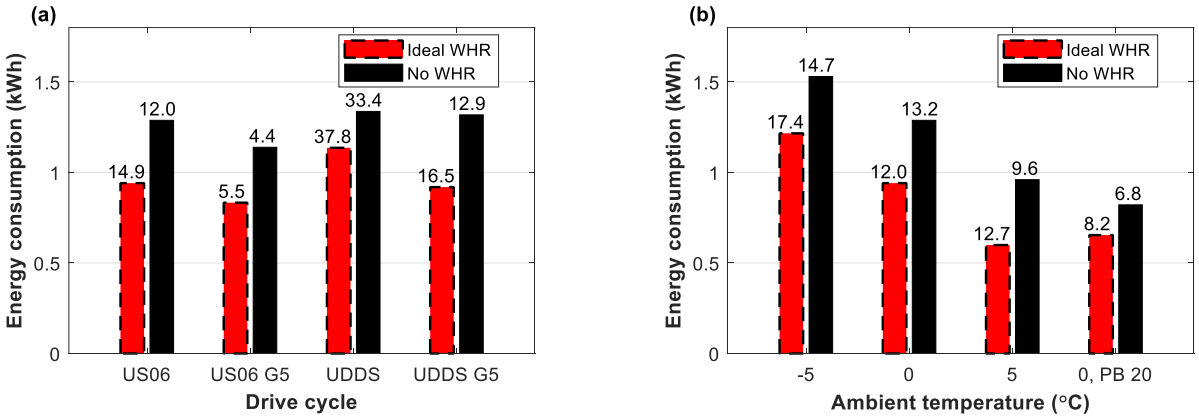

Figure 14. TMS Energy consumption for different (a) drive cycles and grades (T_{amb} = 0°C), (b) ambient temperature and battery preheat state (US06 drive cycle). All cases shown include a heat pump. Numbers on top of the bar graph represent range increase with respect to PTC no WHR configuration. By default, the drive cycle is US06 with a zero grade and battery is not preheated unless stated otherwise (G-grade, PB- preheated battery).

With decreasing ambient temperatures, the EV TMS energy consumption increases as expected to satisfy higher heating requirements. The energy savings decrease because at lower temperatures the DT is cold and takes more time to reach a high enough temperature for WHR activation. The effect on range increase for HP configurations relative to PTC heating increases at lower ambient temperatures because the PTC heater will consume more energy than a HP (since

$COP_{HP} > COP_{PTC}$) to satisfy the same increase in heating load requirements. In the case of a preheated battery, everything else being the same, the TMS energy and savings decrease due to the absence of the need to heat the battery and a reduction in potential usage of WHR respectively. The range increase of HP configurations with respect to PTC also decreases due to lower heating loads. Overall, the range increase of the base HP (no WHR) relative to PTC (no WHR) heating varies from 4.4-33.4% with an extra 1.1-4.4% possible from ideal WHR depending on drive cycle, grade, ambient temperature and battery preheat state.

4.4 Discussion on thermal architecture design and future work

The tradeoffs introduced in the decision tree (Section 3.1, Figure 5) were analyzed with the objective of maximizing system efficiency and performance by comparing factors like energy consumption and heating rates. This helps in figuring out the set of functionalities in the form of component connections, interactions, and control strategy. The GIL framework (Section 3.2) used for the analysis has full freedom to connect the components in any arrangement to analyze various system configurations. Constraints were added by a control algorithm for mode selection to operate valves for analyzing the different WHR configurations. However, in a real system, many physical constraints come into play which restrict the available functionality in a system. The traditional approach of first determining an architecture and then utilizing the connections that it can offer might fail to include the set of functionalities which could otherwise have been more beneficial. It is therefore important to first find the critical functionalities, as done using the GIL framework for modes and WHR configurations analysis, which the system should have to ensure higher efficiency. D2B WHR makes a considerable contribution to energy savings when the battery needs heating whereas D2C WHR offers slightly lower savings, but it does so throughout the cycle run. The B2C WHR configuration will only be useful when the battery heat generation is very large (heavy drive cycles), or it is already preheated to high temperatures (such as after fast charging). Ideal WHR combines all the benefits and acts as the benchmark with the highest system efficiency.

Numerous thermal architectures from leading EV manufacturer patents and existing literature are compared in Table 4 in the context of the decision tree (Figure 5) to show its overall applicability for EV TMS design. The designs are compared by the cabin conditioning type and HP configuration along with the type of WHR the architecture can utilize to offer equivalent or approximately similar physical interactions. Other practical aspects of thermal architecture like

number and type of different HXs, valves and pumps are also compared as a measure of design complexity.

Table 4. Comparison of various thermal architectures in context of the decision tree (Figure 5)

Design	Cabin conditioning	Heat pump configuration	WHR configuration	HXs (2P-MA, 2P-TL, TL-MA)	Valves	Pump	Thermal modes
Tian et al. [9]	Direct	Ref. flow reversal	D2C	5 (2+2+1)	1 *4W* +6 *on-off*	2	5
Kiss et al. [47]	Indirect	Coolant route switching	D2Cab	5 (0+2+3)	8 *3W* + 2 *on-off*	2	4+
Tesla [36]	Direct	Multiple evap. & cond.	D2C+D2B +B2C	5 (2+2+1)	Octovalve +2 *on-off*	2	13
Hyundai [35]	Indirect	Coolant route switching	D2C	7 (0+2+5)	3 *4W*+1 *3W*	4	7

The thermal architecture developed by Tian et al. [9] has direct cabin conditioning and utilizes a 4-way valve for refrigerant flow reversal in the heating mode. The motor waste heat is indirectly recovered via a waste heat recovery HX which increases the suction temperature at compressor inlet leading to a higher system efficiency. The architecture uses a total of five HXs and six on-off valves for coolant line switching and can run on five different thermal modes. Kiss et al. [47] developed an indirect cabin conditioning architecture with direct waste heat recovery from the power electronics and electric motor to the cabin (note that D2Cab, i.e., DT to cabin was excluded from this study because of reasons mentioned in Section 3.3). The system can run in four (or more) modes and has a complex architecture using eight 3-way valves, two on-off valves with five HXs and two pumps. Amongst the leading EV manufacturers, Tesla [36] (Figure 15a) utilizes direct conditioning of the cabin with the HP being configured by means of multiple evaporators and condensers inside the cabin. It can utilize all three D2C, D2B & B2C WHR modes (thus ideal WHR), uses five HXs and two pumps and can operate in thirteen different modes. Hyundai [36] (Figure 15b) uses indirect cabin conditioning and achieves HP operation by switching coolant lines. This makes the coolant side design much more complex with seven HXs, four pumps and three 4-way and one 3-way valve. The architecture can utilize D2C WHR and has seven operating modes.

To switch the coolant lines and operate between different modes it is important to have advanced valves which can cater to specific needs of the system. Tesla developed its own Octovalve (Fig 15a, bottom) whereas Hyundai created an integrated module [34] to replace individual valves for switching connections to operate in different modes (Figure 15b, bottom). This helps in simplifying the design by reducing the number of connections, making the system more modular and compact, and bringing down the overall cost. These designs and custom advanced valves are however very specific in nature, future work will be targeted to develop a generic methodology to come up with an optimized thermal architecture for any given modes and functionalities by minimizing valves, pumps, HXs and coolant routes.

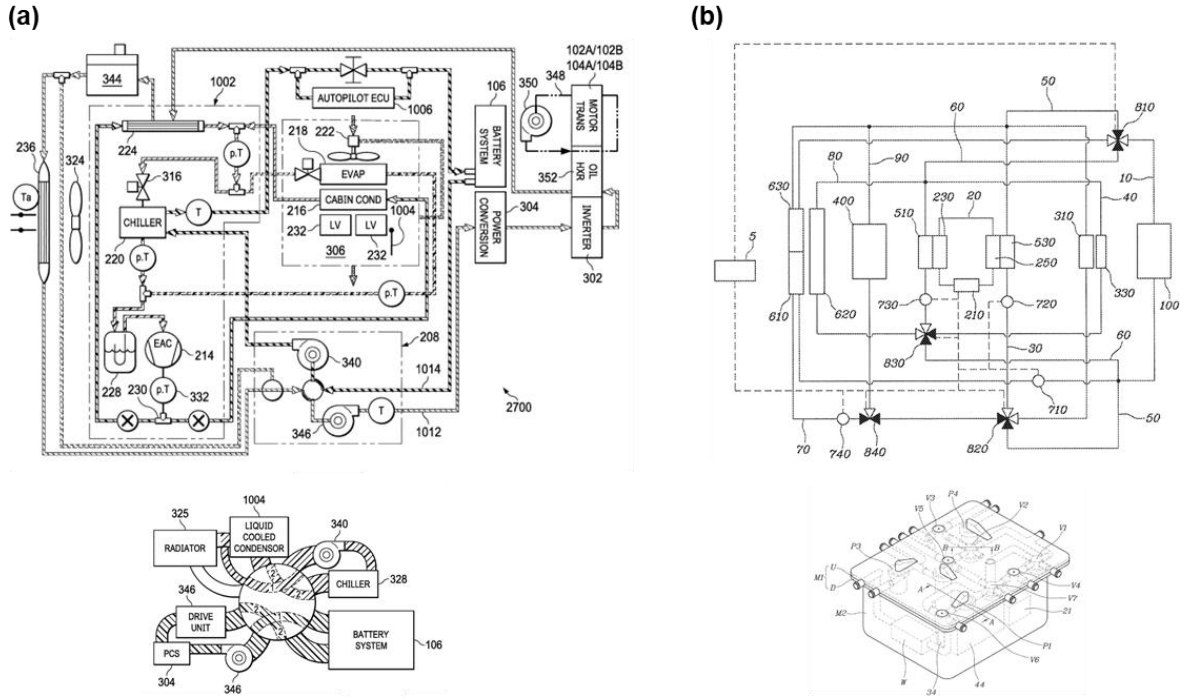

Figure 15. Schematics of the (a) Tesla thermal architecture (top) and Octovalve (bottom) [36]. Schematics of the (b) Hyundai thermal architecture [35] (top) and Integrated Module [34] (bottom). Schematics not to scale. Schematics adapted from Refs [34-36] with permission. Copyright: United States Patent and Trademark Office.

5 CONCLUSIONS

A simulation framework has been created that enables system-level analysis of EV TMS design configurations. Individual component models are developed and integrated together to form the system and validation is done at both the component and system-level. The validated framework is then used to analyze various aspects of a decision tree for the evaluation of EV TMS design trade-offs. The decision tree allows systematic, structured development and assessment of all possible TMS configurations. Its application is also discussed in the context of published TMS architectures developed by other researchers and EV manufacturers.

Direct and indirect configurations for cabin conditioning using heat pump (HP) technologies are analyzed for system performance and the conditioning (heating/cooling) rates. The indirect system is found to have a lower performance with 1.6-1.8x longer cabin conditioning time to reach the desired setpoint temperature when compared to the direct system. The indirect configuration also has a lower efficiency, with reductions in COP ranging from 18-31% and 31-41% for heating and cooling, respectively, when compared to the direct configuration.

A general integrated loop (GIL) is formulated to analyze various EV TMS configurations by changing the control algorithms. This is used to represent an idealized system with all possible operating modes. The system modes are designed to satisfy the thermal constraints of the cabin, drivetrain, and battery for all possible conditions. The system is analyzed for various weather and driving conditions to find the critical set of modes based on their relative occurrence by doing a histogram study. The GIL is also used to simulate various waste heat recovery configurations.

For the US06 (grade 0) drive cycle at an ambient temperature of 0°C, the base version of the HP (no WHR) saves 52.1% TMS energy relative to the PTC heating version resulting in a range increase of 12%. The HP performance increases further with integration of waste heat recovery. Ideal WHR, being the union of all possible WHR modes, gives the highest added TMS energy savings of 12% over the base HP, equating to a 2.9% range increase. Moreover, ideal WHR increases the cabin heating rate by 30.1% relative to no WHR. Ideal WHR is also shown to improve the HP LCC heating capacity by 28.4% at an ambient temperature of -10°C, therefore making HP operation feasible even in very cold conditions.

The TMS energy consumption analysis is repeated for different drive cycles, grades, ambient temperatures, and battery preheat state and the range increase of the base HP (no WHR) relative

to the PTC heating method is found to vary from 4.4-33.4% with an extra 1.1-4.4% possible by using ideal WHR. The UDDS drive cycle in mild conditions (0°C) benefits the most, with a range increase of 33.4% for the base HP implementation, and a 37.8% range increase when using ideal WHR with a HP, showing the importance of HP systems and waste heat recovery for regular urban city driving conditions.

REFERENCES

[1] M. Muratori, M. Alexander, D. Arent, M. Bazilian, E.M. Dede, J. Farrell, C. Gearhart, D. Greene, A. Jenn, M. Keyser, T. Lipman, S. Narumanchi, A. Pesaran, R. Sioshansi, E. Suomalainen, G. Tal, K. Walkowicz, J. Ward, The rise of electric vehicles-2020 status and future expectations, Progress in Energy. 3 (2021). https://doi.org/10.1088/2516-1083/abe0ad.

[2] B. Nykvist, M. Nilsson, Rapidly falling costs of battery packs for electric vehicles, Nat Clim Chang. 5 (2015) 329–332. https://doi.org/10.1038/nclimate2564.

[3] A. Alagumalai, Internal combustion engines: Progress and prospects, Renewable and Sustainable Energy Reviews. 38 (2014) 561–571. https://doi.org/10.1016/j.rser.2014.06.014.

[4] G. Kalghatgi, Is it really the end of internal combustion engines and petroleum in transport?, Appl Energy. 225 (2018) 965–974. https://doi.org/10.1016/j.apenergy.2018.05.076.

[5] H. Liu, M. Wen, H. Yang, Z. Yue, M. Yao, State-of-the-Art Review A Review of Thermal Management System and Control Strategy for Automotive Engines, (2021). https://doi.org/10.1061/(ASCE).

[6] F. Caresana, M. Bilancia, C.M. Bartolini, Numerical method for assessing the potential of smart engine thermal management: Application to a medium-upper segment passenger car, Appl Therm Eng. 31 (2011) 3559–3568. https://doi.org/10.1016/j.applthermaleng.2011.07.017.

[7] Z. Tian, B. Gu, W. Gao, Y. Zhang, Performance evaluation of an electric vehicle thermal management system with waste heat recovery, Appl Therm Eng. 169 (2020). https://doi.org/10.1016/j.applthermaleng.2020.114976.

[8] H. Min, Z. Zhang, W. Sun, Z. Min, Y. Yu, B. Wang, A thermal management system control strategy for electric vehicles under low-temperature driving conditions considering battery lifetime, Appl Therm Eng. 181 (2020). https://doi.org/10.1016/j.applthermaleng.2020.115944.

[9] Z. Tian, W. Gan, X. Zhang, B. Gu, L. Yang, Investigation on an integrated thermal management system with battery cooling and motor waste heat recovery for electric vehicle, Appl Therm Eng. 136 (2018) 16–27. https://doi.org/10.1016/j.applthermaleng.2018.02.093.

[10] Z. Tian, B. Gu, Analyses of an integrated thermal management system for electric vehicles, Int J Energy Res. 43 (2019) 5788–5802. https://doi.org/10.1002/er.4679.

[11] T. Rana, Y. Yamamoto, Universal electric vehicle thermal management system, in: SAE Technical Papers, SAE International, 2020. https://doi.org/10.4271/2020-28-0002.

[12] T.T. Wang, A. Jagarwal, J.R. Wagner, G. Fadel, Optimization of an Automotive Radiator Fan Array Operation to Reduce Power Consumption, IEEE/ASME Transactions on Mechatronics. 20 (2015) 2359–2369. https://doi.org/10.1109/TMECH.2014.2377655.

[13] S.C. Pang, M.A. Kalam, H.H. Masjuki, M.A. Hazrat, A review on air flow and coolant flow circuit in vehicles' cooling system, Int J Heat Mass Transf. 55 (2012) 6295–6306. https://doi.org/10.1016/j.ijheatmasstransfer.2012.07.002.

[14] Q.L. Yue, C.X. He, M.C. Wu, T.S. Zhao, Advances in thermal management systems for next-generation power batteries, Int J Heat Mass Transf. 181 (2021). https://doi.org/10.1016/j.ijheatmasstransfer.2021.121853.

[15] J. Lin, X. Liu, S. Li, C. Zhang, S. Yang, A review on recent progress, challenges and perspective of battery thermal management system, Int J Heat Mass Transf. 167 (2021). https://doi.org/10.1016/j.ijheatmasstransfer.2020.120834.

[16] W. Zichen, D. Changqing, A comprehensive review on thermal management systems for power lithium-ion batteries, Renewable and Sustainable Energy Reviews. 139 (2021). https://doi.org/10.1016/j.rser.2020.110685.

[17] Q. Wang, B. Jiang, B. Li, Y. Yan, A critical review of thermal management models and solutions of lithium-ion batteries for the development of pure electric vehicles, Renewable and Sustainable Energy Reviews. 64 (2016) 106–128. https://doi.org/10.1016/j.rser.2016.05.033.

[18] W. Wu, S. Wang, W. Wu, K. Chen, S. Hong, Y. Lai, A critical review of battery thermal performance and liquid based battery thermal management, Energy Convers Manag. 182 (2019) 262–281. https://doi.org/10.1016/j.enconman.2018.12.051.

[19] B. Chidambaranathan, M. Vijayaram, V. Suriya, R. Sai Ganesh, S. Soundarraj, A review on thermal issues in Li-ion battery and recent advancements in battery thermal management system, in: Mater Today Proc, Elsevier Ltd, 2020: pp. 116–128. https://doi.org/10.1016/j.matpr.2020.03.317.

[20] A. Tomaszewska, Z. Chu, X. Feng, S. O'Kane, X. Liu, J. Chen, C. Ji, E. Endler, R. Li, L. Liu, Y. Li, S. Zheng, S. Vetterlein, M. Gao, J. Du, M. Parkes, M. Ouyang, M. Marinescu, G. Offer, B. Wu, Lithium-ion battery fast charging: A review, ETransportation. 1 (2019). https://doi.org/10.1016/j.etran.2019.100011.

[21] M. Keyser, A. Pesaran, Q. Li, S. Santhanagopalan, K. Smith, E. Wood, S. Ahmed, I. Bloom, E. Dufek, M. Shirk, A. Meintz, C. Kreuzer, C. Michelbacher, A. Burnham, T. Stephens, J. Francfort, B. Carlson, J. Zhang, R. Vijayagopal, K. Hardy, F. Dias, M. Mohanpurkar, D. Scoffield, A.N. Jansen, T. Tanim, A. Markel, Enabling fast charging – Battery thermal considerations, J Power Sources. 367 (2017) 228–236. https://doi.org/10.1016/j.jpowsour.2017.07.009.

[22] J. Kim, J. Oh, H. Lee, Review on battery thermal management system for electric vehicles, Appl Therm Eng. 149 (2019) 192–212. https://doi.org/10.1016/j.applthermaleng.2018.12.020.

[23] C. Vidal, O. Gross, R. Gu, P. Kollmeyer, A. Emadi, XEV Li-Ion Battery Low-Temperature Effects-Review, IEEE Trans Veh Technol. 68 (2019) 4560–4572. https://doi.org/10.1109/TVT.2019.2906487.

[24] J. Jaguemont, L. Boulon, Y. Dubé, A comprehensive review of lithium-ion batteries used in hybrid and electric vehicles at cold temperatures, Appl Energy. 164 (2016) 99–114. https://doi.org/10.1016/j.apenergy.2015.11.034.

[25] A. Yokoyama, T. Osaka, Y. Imanishi, S. Sekiya, Thermal Management System for Electric Vehicles, Source: SAE International Journal of Materials and Manufacturing. 4 (2011) 1277–1285. https://doi.org/10.2307/26273859.

[26] D. Ramsey, A. Bouscayrol, L. Boulon, A. Vaudrey, Simulation of an electric vehicle to study the impact of cabin heating on the driving range, 2020 IEEE 91st Vehicular Technology Conference (VTC2020-Spring). (2020). https://doi.org/10.1109/VTC2020-Spring48590.2020.9129169.

[27] J.T. Lee, S. Kwon, Y. Lim, M.S. Chon, D. Kim, Effect of air-conditioning on driving range of electric vehicle for various driving modes, in: SAE Technical Papers, SAE International, 2013. https://doi.org/10.4271/2013-01-0040.

[28] S. Chowdhury, L. Leitzel, M. Zima, M. Santacesaria, G. Titov, J. Lustbader, J. Rugh, J. Winkler, A. Khawaja, M. Govindarajalu, Total Thermal Management of Battery Electric Vehicles (BEVs), in: SAE Technical Papers, SAE International, 2018. https://doi.org/10.4271/2018-37-0026.

[29] Z. Zhang, D. Wang, C. Zhang, J. Chen, Electric vehicle range extension strategies based on improved AC system in cold climate – A review, International Journal of Refrigeration. 88 (2018) 141–150. https://doi.org/10.1016/j.ijrefrig.2017.12.018.

[30] D. Yang, Y. Huo, Q. Zhang, J. Xie, Z. Yang, Recent advances on air heating system of cabin for pure electric vehicles: A review, Heliyon. 8 (2022). https://doi.org/10.1016/j.heliyon.2022.e11032.

[31] Z. Qi, Advances on air conditioning and heat pump system in electric vehicles - A review, Renewable and Sustainable Energy Reviews. 38 (2014) 754–764. https://doi.org/10.1016/j.rser.2014.07.038.

[32] Z. Zhang, J. Wang, X. Feng, L. Chang, Y. Chen, X. Wang, The solutions to electric vehicle air conditioning systems: A review, Renewable and Sustainable Energy Reviews. 91 (2018) 443–463. https://doi.org/10.1016/j.rser.2018.04.005.

[33] F. Qin, Q. Xue, G.M.A. Velez, G. Zhang, H. Zou, C. Tian, Experimental investigation on heating performance of heat pump for electric vehicles at -20 °C ambient temperature,

Energy Convers Manag. 102 (2015) 39–49. https://doi.org/10.1016/j.enconman.2015.01.024.

[34] M.J. Oh, S.S. Lee, J.W. Kim, S. la Chung, Y.S. Chung, G.B. Choi, US Patent No. US11192425B2, 2021.

[35] M.J. Oh, J.W. Kim, S.S. Lee, US Patent No. US10766338B2, 2020.

[36] N. Mancini, J.S.M. Mardall, J. Kopitz, C.R. O'Donnell, D.F. Hanks, H. Li, US Patent No. US20190070924A1, 2019.

[37] S. Lee, Y. Chung, Y. Jeong, M.S. Kim, Experimental study on an electric vehicle heat pump system with multi-level waste heat recovery using a vapor injection technique at low ambient temperatures, Energy Convers Manag. 267 (2022). https://doi.org/10.1016/j.enconman.2022.115935.

[38] C. Kwon, M.S. Kim, Y. Choi, M.S. Kim, Performance evaluation of a vapor injection heat pump system for electric vehicles, International Journal of Refrigeration. 74 (2017) 136–148. https://doi.org/10.1016/j.ijrefrig.2016.10.004.

[39] F. Qin, Q. Xue, G.M.A. Velez, G. Zhang, H. Zou, C. Tian, Experimental investigation on heating performance of heat pump for electric vehicles at -20 °C ambient temperature, Energy Convers Manag. 102 (2015) 39–49. https://doi.org/10.1016/j.enconman.2015.01.024.

[40] J. Jung, Y. Jeon, H. Lee, Y. Kim, Numerical study of the effects of injection-port design on the heating performance of an R134a heat pump with vapor injection used in electric vehicles, Appl Therm Eng. 127 (2017) 800–811. https://doi.org/10.1016/j.applthermaleng.2017.08.098.

[41] A.J. Mahvi, K. Boyina, A. Musser, S. Elbel, N. Miljkovic, Superhydrophobic heat exchangers delay frost formation and enhance efficency of electric vehicle heat pumps, Int J Heat Mass Transf. 172 (2021). https://doi.org/10.1016/j.ijheatmasstransfer.2021.121162.

[42] S.H. Hong, D.S. Jang, S. Yun, J.H. Baek, Y. Kim, Performance improvement of heat pumps using novel microchannel heat exchangers with plain-louver fins during periodic frosting and defrosting cycles in electric vehicles, Energy Convers Manag. 223 (2020). https://doi.org/10.1016/j.enconman.2020.113306.

[43] Y.M. Alkhulaifi, N.A.A. Qasem, S.M. Zubair, Improving the performance of thermal management system for electric and hybrid electric vehicles by adding an ejector, Energy Convers Manag. 201 (2019). https://doi.org/10.1016/j.enconman.2019.112133.

[44] H. Zou, T. Yang, M. Tang, C. Tian, D. Butrymowicz, Ejector optimization and performance analysis of electric vehicle CO2 heat pump with dual ejectors, Energy. 239 (2022). https://doi.org/10.1016/j.energy.2021.122452.

[45] J. Wu, G. Zhou, M. Wang, A comprehensive assessment of refrigerants for cabin heating and cooling on electric vehicles, Appl Therm Eng. 174 (2020). https://doi.org/10.1016/j.applthermaleng.2020.115258.

[46] B. Yu, J. Yang, D. Wang, J. Shi, J. Chen, Energy consumption and increased EV range evaluation through heat pump scenarios and low GWP refrigerants in the new test procedure WLTP, International Journal of Refrigeration. 100 (2019) 284–294. https://doi.org/10.1016/j.ijrefrig.2019.01.033.

[47] T. Kiss, J. Lustbader, D. Leighton, Modeling of an Electric Vehicle Thermal Management System in MATLAB/Simulink, in: SAE Technical Papers, SAE International, 2015. https://doi.org/10.4271/2015-01-1708.

[48] D. Leighton, Combined Fluid Loop Thermal Management for Electric Drive Vehicle Range Improvement, SAE International Journal of Passenger Cars - Mechanical Systems. 8 (2015) 711–720. https://doi.org/10.4271/2015-01-1709.

[49] S. Singh, M. Jennings, S. Katragadda, J. Che, N. Miljkovic, MATLAB-Simulink-Simscape Model with Simulation data for Electric Vehicle Thermal Management System, Mendeley Data. v1 (2023). https://doi.org/10.17632/d26h5dn2z7.1.

[50] E.S. Islam, A. Moawad, N. Kim, A. Rousseau, Energy Consumption and Cost Reduction of Future Light-Duty Vehicles through Advanced Vehicle Technologies: A Modeling Simulation Study Through 2050, United States, 2020. https://doi.org/10.2172/1647165.